

# 拉萨地体南缘桑日地区晚白垩世火山岩的年代学、 岩石地球化学及成因

杨同山<sup>1)</sup>, 郎兴海<sup>1)\*</sup>, 王旭辉<sup>1)</sup>, 邓煜霖<sup>1)</sup>, 吕 娜<sup>1)</sup>,  
董 咪<sup>1)</sup>, 何 青<sup>1)</sup>, 张相国<sup>2)</sup>, 梁海辉<sup>1)</sup>

1)成都理工大学地球科学学院, 四川成都 610059;

2)西藏自治区地质矿产开发局区域地质调查大队, 西藏拉萨 851400

**摘要:** 拉萨地体南缘桑日地区中酸性火山岩出露广泛, 多期次岩浆活动的叠加使得区内岩浆岩成分复杂、形成时代跨度大。为深入研究该地区火山岩的形成时代、构造背景和成因机制, 本文选取桑日县西侧塔木村附近的中酸性火山岩为研究对象, 开展锆石 U-Pb 定年、全岩主微量及 Sr-Nd 同位素分析。锆石 U-Pb 年龄表明桑日地区塔木村火山岩形成于 91.7~90.8 Ma, 属于晚白垩世。桑日地区晚白垩世火山岩 SiO<sub>2</sub> 含量为 55.79%~74.26%, MgO 含量为 1.31%~4.34%, 同时具有高 Sr(平均含量为  $779 \times 10^{-6}$ )、低 Y( $8.36 \times 10^{-6}$ ~ $15.85 \times 10^{-6}$ )、Yb( $0.92 \times 10^{-6}$ ~ $1.38 \times 10^{-6}$ )含量及高 Sr/Y 比值(36.28~105.59)的特征, 表明桑日晚白垩世火山岩为埃达克质岩石。同时该地区晚白垩世火山岩富集大离子亲石元素 Rb、Sr 和 Pb, 亏损高场强元素 Nb、Ta 和 Ti, 具有较低的  $^{87}\text{Sr}/^{86}\text{Sr}$  初始值(0.704 152~0.704 515)和较高的  $^{143}\text{Nd}/^{144}\text{Nd}$  初始值(0.512 676~0.512 750)。综合岩石地球化学特征和区域地质资料, 桑日地区晚白垩世火山岩形成于新特提斯洋壳北向俯冲消减有关的活动大陆边缘环境, 是新特提斯洋壳部分熔融的产物, 洋壳熔体上升过程中伴有地幔楔物质的加入并经历了分离结晶作用。

**关键词:** 拉萨地体南缘; 桑日地区; 晚白垩世; 新特提斯洋; 火山岩

中图分类号: P588.14; P534.53 文献标志码: A doi: 10.3975/cagsb.2022.032801

## Chronology, Geochemical Characteristics, and Genesis of Late Cretaceous Volcanic Rocks in Sangri Area, Southern Margin of the Lhasa Terrane

YANG Tong-shan<sup>1)</sup>, LANG Xing-hai<sup>1)\*</sup>, WANG Xu-hui<sup>1)</sup>, DENG Yu-lin<sup>1)</sup>, LÜ Na<sup>1)</sup>, DONG Mi<sup>1)</sup>, HE Qing<sup>1)</sup>, ZHANG Xiang-guo<sup>2)</sup>, LIANG Hai-hui<sup>1)</sup>

1) College of Earth Sciences, Chengdu University of Technology, Chengdu, Sichuan 610059;

2) Regional Geological Survey Party, Tibet Bureau of Geology and Mineral Resources Exploration and Development, Lhasa, Tibet 851400

**Abstract:** Intermediate-acid volcanic rocks are widely exposed in the Sangri area of the southern margin of Lhasa terrane. The superposition of multiple magmatic activities over a long formation time has made the composition of magmatic rocks in the area complex. To study the formation age, tectonic setting, and genetic mechanism of volcanic rocks in this area, we selected the intermediate-acid volcanic rocks near Tamu Village in the west of

本文由四川省科技计划项目(编号: 2020JDJQ0042)、国家自然科学基金(编号: 41502079; 41972084)、国家重点研发计划课题(编号: 2018YFC0604105)、成都理工大学珠峰科学研究计划(编号: 2020ZF11047)、西北大学大陆动力学国家重点实验室开放基金(编号: 18LCD04)、自然资源部深地资源成矿作用与矿产预测重点实验室开放基金(编号: ZS1911)和中国地质调查局项目(编号: DD20190167; DD20160346)联合资助。

收稿日期: 2022-01-20; 改回日期: 2022-03-23; 网络首发日期: 2022-03-31。责任编辑: 闫立娟。

第一作者简介: 杨同山, 男, 1994 年生。硕士研究生。研究方向为岩石学。E-mail: 879845285@qq.com。

\*通讯作者: 郎兴海, 男, 1982 年生。博士, 教授。主要从事岩石学及矿床学方向的研究。E-mail: langxinghai@126.com。

Sangri County as the research object, conducted zircon U-Pb dating, and analyzed whole rock major and trace elements and Sr-Nd isotopes. The SiO<sub>2</sub> and MgO contents in Late Cretaceous volcanic rocks in the Sangri area were 55.79%~74.26% and 1.31%~4.34%, respectively. In addition, they have high Sr (average  $779 \times 10^{-6}$ ), low Y ( $8.36 \sim 15.85 \times 10^{-6}$ ) and Yb ( $0.92 \sim -1.38 \times 10^{-6}$ ), and a high Sr/Y ratio (36.28~05.59). Geochemical characteristics showed that the Late Cretaceous volcanic rocks in the Sangri area are adakite rocks. Moreover, the Late Cretaceous Sangri volcanic rocks are enriched in large ion lithophile elements (LILE), such as Rb, Sr, and Pb, and depleted in high field strength elements (HFSE), such as Nb, Ta, and Ti, with low initial values of  $^{87}\text{Sr}/^{86}\text{Sr}$  (0.704 152~0.704 515) and high initial values of  $^{143}\text{Nd}/^{144}\text{Nd}$  (0.512 676~0.512 750). Based on petrogeochemical characteristics and regional geological data, the Late Cretaceous volcanic rocks in the Sangri area formed in an active continental margin environment related to the northward subduction of the Neo-Tethyan oceanic crust and were produced by the partial melting of the Neo-Tethyan oceanic crust. The rising process of ocean crust melting was accompanied by the addition of mantle wedge material, which led to fractional crystallization.

**Key words:** southern margin of the Lhasa Terrane; Sangri area; Late Cretaceous; Neo-Tethys ocean; volcanic rocks

位于青藏高原中部的拉萨地体，东西向延伸约2500 km，南北向跨度150~300 km，是一条超大型的岩浆-构造带(Chung et al., 2003, 2005; Mo et al., 2005, 2007; 潘桂棠等, 2006)。拉萨地体南缘广泛分布着自古生代至新生代的岩浆岩，蕴藏着与特提斯洋和青藏高原演化相关的地质记录，是研究洋壳俯冲和陆陆碰撞的天然实验室(莫宣学等, 2005; He et al., 2020; Yang et al., 2021; Li et al., 2021)。

拉萨地体南缘是整个拉萨地体中岩浆活动最为活跃的地区(潘桂棠等, 2006; 张泽明等, 2019; Ran et al., 2019)。其岩浆活动可划分为五期： $\sim 370$ ~ $340$  Ma、 $\sim 220$ ~ $152$  Ma、 $\sim 109$ ~ $80$  Ma、 $\sim 65$ ~ $41$  Ma、 $\sim 33$ ~ $13$  Ma(莫宣学等, 2005; Wen et al., 2008a, b; Ji et al., 2009; Wang et al., 2020)。前人研究认为，第一期的岩浆作用与晚古生代拉萨地体的裂解过程有关(Wang et al., 2020)；第二、三期的岩浆活动主要与新特提斯洋的北向俯冲有关，记录了洋壳在俯冲消减过程中的动力学机制(潘桂棠等, 2006; Lang et al., 2018, 2019, 2020; Wang et al., 2019)；第四、五期的岩浆活动记录了印度大陆和欧亚大陆从初始碰撞到后碰撞的过程(莫宣学等, 2003, 2005; 侯增谦等, 2006; 王旭辉等, 2019)。

桑日地区自晚古生代以来，先后经历了新特提斯洋开启、俯冲消减、消亡及印亚大陆碰撞的演化过程(Yin and Harrison, 2000; 潘桂棠等, 2006; 许志琴等, 2011; Zhu et al., 2011, 2013)，多期次岩浆活动的叠加使得区内岩浆作用复杂，岩石形成时代跨度大，火山岩地层时代归属问题争议多。桑日地区出露的火山岩地层主要有麻木下组、旦师庭组和比马组。近十余年来，前人开展了年代学研究，得到了多组火山岩锆石U-Pb年龄(图1c)，初步构建了区域中生代火山岩的年代学格架：Zhu et al.(2009)和康志强等(2015)对马门附近的麻木下组火山岩进行了年代学研究，得到其锆石U-Pb年龄为136~

100 Ma，属于早白垩世；康志强等(2015)和Ran et al.(2019)在旦师庭庙附近获得了晚白垩世旦师庭组火山岩的锆石U-Pb年龄(97~90 Ma)，表明其形成于晚白垩世。而前人在不同地区获得的比马组火山岩年代学数据差别较大：Kang et al.(2014)在桑日县卡马档附近比马组火山岩获得了早侏罗世锆石U-Pb年龄(195~189 Ma)；闫国强等(2014)在山南努日矿区比马组安山岩获得了晚白垩世的锆石U-Pb年龄(92.0 Ma)。因此，有必要对比马组火山岩的形成时代作进一步细化研究，完善桑日地区火山岩的年代学格架。

火山岩的形成时代对于研究其演化过程具有重要作用，正确厘定火山岩年龄，是研究其构造背景和成因机制的基础。因此，本文选取桑日地区塔木村东侧比马组火山岩为研究对象，开展锆石U-Pb年代学、全岩主微量元素及Sr-Nd同位素分析，综合前人研究成果，厘定地层时代，探讨该火山岩的成因和构造背景，以期完善拉萨地体南缘比马组火山岩的研究。

## 1 区域地质概况和样品采集

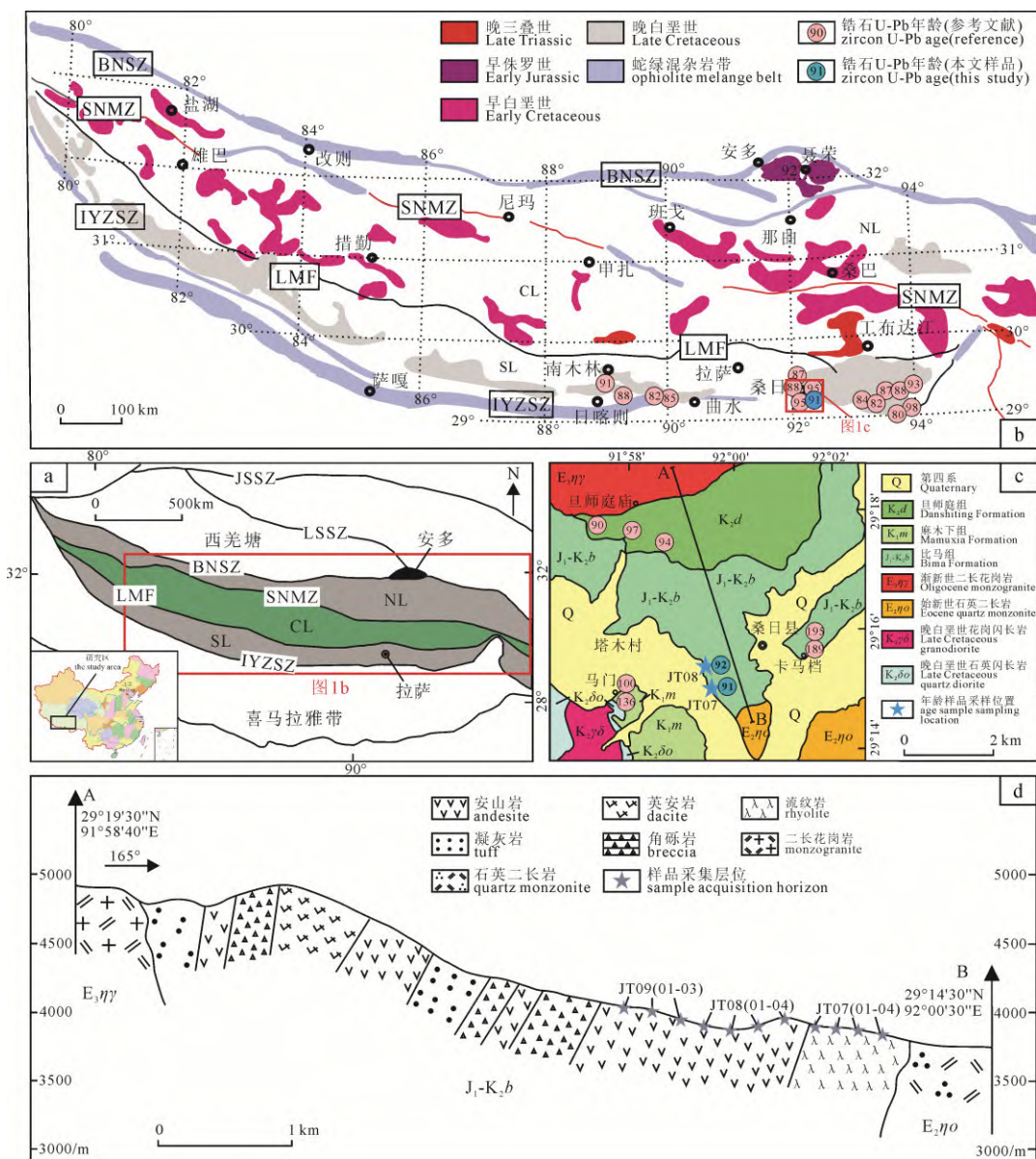
青藏高原自北向南由多个微陆块拼接而成，依次是松潘—甘孜地体、羌塘地体、拉萨地体和喜马拉雅地体(Yin and Harrison, 2000)(图1a)。其中，拉萨地体北以班公湖—怒江缝合带(BNSZ)为界，南以印度—雅鲁藏布江缝合带(IYZSZ)为界(图1a)，东西向延伸近2000 km，南北向跨度约300 km，是青藏高原岩浆活动最活跃的地区之一，广泛分布着不同时代的岩浆岩。在拉萨地体内部，以狮泉河—纳木错蛇绿混杂岩带(SNMZ)和洛巴堆—米拉山断裂带(LMF)为界，由北向南将拉萨地体分为北部拉萨地体(NL)、中部拉萨地体(CL)和南部拉萨地体(SL)(图1b)。

桑日地区的火山岩分布在南部拉萨地体中东

段南缘(图 1b), 紧邻雅鲁藏布江缝合带的北侧, 主要由安山岩-英安质熔岩-碎屑熔岩-火山碎屑岩组成, 桑日地区出露的中生代火山岩地层主要包括麻木下组、旦师庭组和比马组。出露的侵入岩以中性和酸性岩为主, 主要有晚白垩世石英闪长岩、晚白垩世花岗闪长岩和渐新世二长花岗岩等(图 1c)。

研究区出露的中生代火山岩地层主要包括麻木下组、旦师庭组和比马组。麻木下组位于研究区西南部(图 1c), 出露面积较小, 岩性主要以安山岩

为主, 夹英安岩并共生大量的沉积火山角砾岩。旦师庭组位于研究区北部(图 1c), 是一套以中性-酸性的火山岩、火山碎屑岩为主的地层, 偶夹杂砂岩。研究区出露的比马组火山岩主要为一套中性-酸性火山熔岩、安山质火山碎屑岩夹少量的沉积岩的岩石组合, 与下部麻木下组呈整合接触。岩层整体呈北西走向, 出露面积约 15 km<sup>2</sup>, 倾角 40°~65°。区域上厚度稳定, 火山岩厚度为 1600~1800 m。本文采集的火山岩样品位于桑日县城西侧塔木村东南



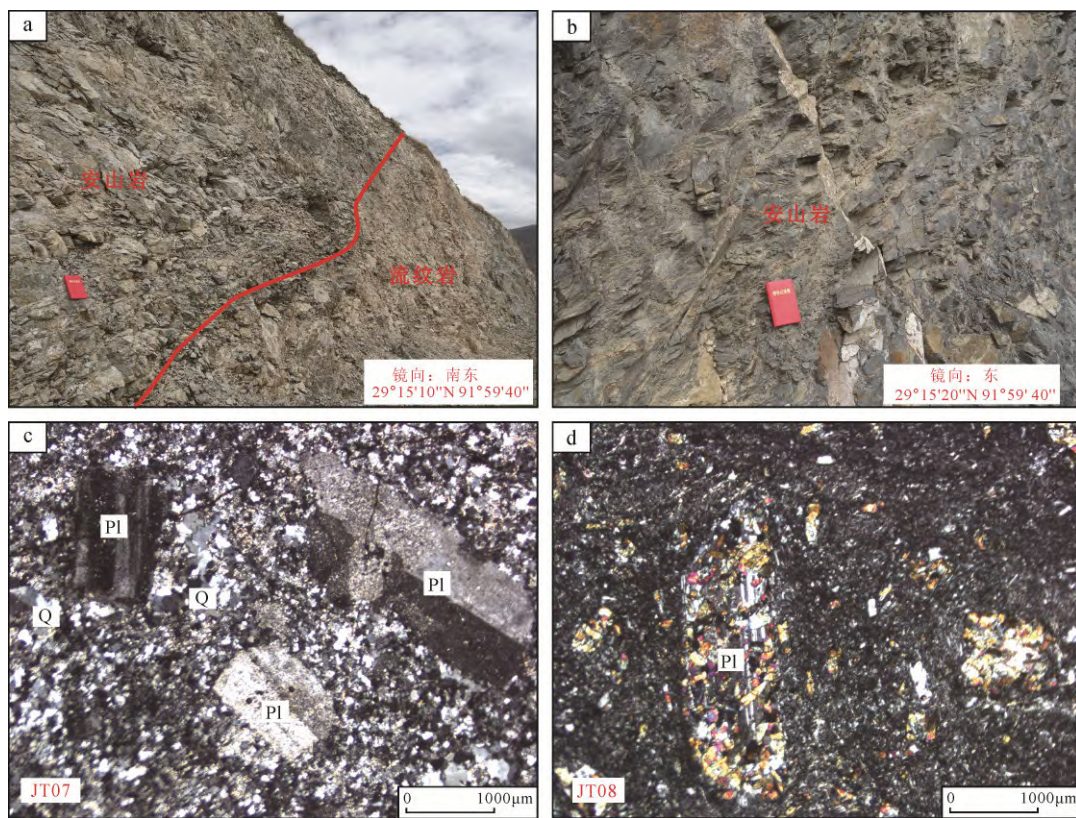
JSSZ—金沙江缝合带; BNSZ—班公湖—怒江缝合带; SNMZ—狮泉河—纳木错蛇绿岩混杂岩带; LMF—洛巴堆—米拉山断裂带;

IYZSZ—印度河—雅鲁藏布缝合带; NL—北部拉萨地体; CL—中部拉萨地体; SL—南部拉萨地体。

JSSZ—Jinshajiang suture zone; BNSZ—Bangong—Nujiang suture zone; SNMZ—Shiquan River—Nam Tso Melange zone; LMF—Luobadui—Milashan Fault; IYZSZ—India River—Yarlung Zangbo suture zone; NL—Northern Lhasa Subterrane; CL—Central Lhasa Subterrane; SL—Northern Lhasa Subterrane.

图 1 青藏高原地质简图(a)、拉萨地体中—新生带岩浆活动划分图(b)、研究区地质简图(c)和 A—B 剖面图(d)  
(a, b 据 Zhu et al., 2009; c, d 据西藏自治区地质调查院, 2018a, b; 年龄数据引自康志强等, 2015; Zhang et al., 2018 及其所引用的文献)

**Fig. 1** Geological map of the Qinghai-Tibet Plateau (a), Mesozoic-Cenozoic magmatic activity distribution map of Lhasa terrane (b), geological sketch of the study area (c), and a geological section at line A-B (d) (a and b, after Zhu et al., 2009; c and d, modified from the Geological Survey of Tibet Autonomous Region, 2018a, b; age data were quoted from KANG et al., 2015; Zhang et al., 2018, and other references)



a, b—桑日地区晚白垩世火山岩野外照片; c—流纹岩镜下显微照片; d—安山岩镜下显微照片(c, d 均为正交偏光); Pl—斜长石; Q—石英。  
a, b—field photos of Late Cretaceous volcanic rocks in Sangri area; c—micrograph of rhyolite under microscope;  
d—images of andesite under a microscope; Pl—plagioclase; Q—quartz.

图 2 桑日地区晚白垩世火山岩野外照片(a, b)和镜下显微照片(c, d)

Fig. 2 Field photographs (a, b) and microscope photos (c, d) of Late Cretaceous volcanic rocks in the Sangri area

侧的比马组, 岩性为中酸性岩, 野外剖面观察到安山岩与流纹岩互层(图 1d)。本文选取新鲜样品 11 件开展全岩地球化学分析, 2 件样品用于锆石 U-Pb 定年, 4 件样品开展 Sr-Nd 同元素分析。

## 2 样品特征与分析方法

流纹岩样品呈现灰色, 具斑状结构, 岩石由斑晶(30%~35%)和基质(65%~70%)组成, 斑晶主要为斜长石和石英, 斜长石具宽板状和板状的轮廓, 粒径长 0.5~2.5 mm, 宽 0.5~1 mm, 部分斜长石表面被绢云母化, 见有较多的溶蚀麻点, 边部见溶蚀反应边; 石英呈不规则粒状, 晶面多亮净, 不均匀分布; 云母呈片状, 颗粒细小, 含量较少; 基质由细小的长石、石英集合体组成, 含有锆石、磁铁矿等副矿物(图 2c)。安山岩样品颜色为灰绿色, 具斑状结构, 斑晶主要为斜长石和暗色矿物, 斜长石为自形棱边平直的宽板状, 聚片双晶发育, 基质由微晶斜长石和角闪石组成(图 2d)。

锆石 U-Pb 年龄测试工作在中国地质科学院矿产资源研究所成矿作用与资源评价重点实验室进行, 仪器为 Neptune 型激光多接收等离子体质谱(LA-MC-ICPMS), 激光剥蚀斑束直径为 25 μm, 以

氦气作为剥蚀锆石颗粒的载气。锆石年龄的计算以国际通用标准锆石 91500 和澳大利亚锆石 GJ-1 为外标。为提高分析精度, 每测 10 个样品点, 开头和结尾分别测量两次 GJ-1 和一次锆石标准样品 Plesovice。后期使用 ICPMSDataCal 软件对被测锆石同位素比值进行处置(Liu et al., 2010), 锆石 U-Pb 年龄结果计算使用 Isoplot 软件完成。

主、微量元素的分析工作在南京聚谱检测科技有限公司进行。选取新鲜样品去除风化面, 将新鲜样品无污染的碎样至 200 目用于元素分析。主量元素采用 XRF 法分析, 分析精度优于 5%。微量元素采用 ICP-MS 方法进行分析。首先将样品粉末倒入杯中, 经过加酸、蒸干、定容等一系列工序, 最后将处理好的样品送到 ICP-MS 仪器室测量所需的微量元素。微量元素含量大于  $10 \times 10^{-6}$  的元素分析误差小于 5%, 而微量元素含量小于  $10 \times 10^{-6}$  的元素分析误差小于 10%。

Sr-Nd 同位素化学前处理与质谱测定在南京聚谱检测科技有限公司完成。测试样品经过酸溶、密封蒸干、分离等制备过程, 在 Nu Plasma II MC-ICP-MS 上测定 Sr-Nd 同位素比值。测试过程中, 以美国地质调查局 USGS 地球化学标准岩石粉末作

为质控盲样, 采用  $^{86}\text{Sr}/^{88}\text{Sr}=0.119\ 4$  和  $^{146}\text{Nd}/^{144}\text{Nd}=0.721\ 9$  进行质量分馏和标准化校正。经过以上处理和测定,  $^{87}\text{Sr}/^{86}\text{Sr}$  值为  $0.704\ 418\sim0.704\ 948$ ,  $^{143}\text{Nd}/^{144}\text{Nd}$  值为  $0.512\ 734\sim0.512\ 809$ , 在误差范围内与 Weis et al.(2006) 报道值吻合。

### 3 分析结果

#### 3.1 锆石 U-Pb 年龄

本文分别对流纹岩样品(JT07-1)和安山岩样品(JT08-1)进行了锆石 U-Pb 定年, 结果见附表 1。流纹岩样品锆石多为自形-半自形短柱状, 颗粒长径在  $50\sim150\ \mu\text{m}$  之间, 长宽比大多数在 1~2 之间, 颜色较深, 颗粒较完整, 部分锆石样品局部破损。锆石阴极发光(CL)图像显示被测锆石具有较为明显的环带结构。安山岩样品锆石多为自形-半自形圆柱状, 粒径介于  $100\sim300\ \mu\text{m}$ , 长宽比大多数在 1~3 之间变化, 颜色较浅, 表面光滑, 大部分锆石样品局部破损, 环带特征不如 JT07-1 样品锆石明显。两组被测锆石样品 Th/U 值变化于 0.95~4.37 之间, 较高的 Th/U 值指示被测锆石都属于岩浆成因锆石(Corfu et al., 2003; Wu and Zheng, 2004)。

流纹岩样品共获得 18 个有效分析测试点数据, 它们的  $^{206}\text{Pb}/^{238}\text{U}$  年龄介于  $95.7\sim87.3\text{ Ma}$  之间, 加权

平均年龄为  $(90.8\pm1.1)\text{ Ma}(\text{MSWD}=0.71)$ (图 3a, b)。安山岩样品共获得 18 个有效分析测试点数据, 它们的  $^{206}\text{Pb}/^{238}\text{U}$  年龄介于  $96.3\sim90.2\text{ Ma}$  之间, 加权平均年龄为  $(91.7\pm1.1)\text{ Ma}(\text{MSWD}=0.25)$ (图 3c, d)。综上所述, 研究样品形成于晚白垩世时期。

#### 3.2 岩石地球化学特征

桑日地区晚白垩世火山岩样品主微量元素分析结果见附表 2。由于样品烧失量较高(1.35~4.36), 因此将扣除分析数据的烧失量, 重新换算到 100%。如图 4 所示, 该火山岩样品大部分落在安山岩和流纹岩区域中。

#### 3.2.1 主量元素

桑日地区晚白垩世安山岩样品  $\text{SiO}_2$  的含量介于 55.79%~64.04% 之间(平均 58.93%),  $\text{Al}_2\text{O}_3$  的含量介于 16.29%~19.19% 之间(平均 17.96%),  $\text{MgO}$  的含量为 3.07%~4.34%(平均 3.50%),  $\text{Mg}^{\#}$  值为 48.60~52.88(平均 50.57),  $\text{K}_2\text{O}$  的含量为 1.24%~2.77%(平均 2.15%),  $\text{Na}_2\text{O}$  的含量为 2.32%~5.46%(平均 3.89%) 及较低的  $\text{K}_2\text{O}/\text{Na}_2\text{O}$  比值(平均 0.63), 属于钙碱性系列岩石(图 5)。

桑日地区晚白垩世流纹岩样品  $\text{SiO}_2$  的含量介于 70.42%~74.26% 之间(平均 72.54%),  $\text{Al}_2\text{O}_3$  的含量介于 12.75%~16.79% 之间(平均 14.63%),  $\text{MgO}$  的含

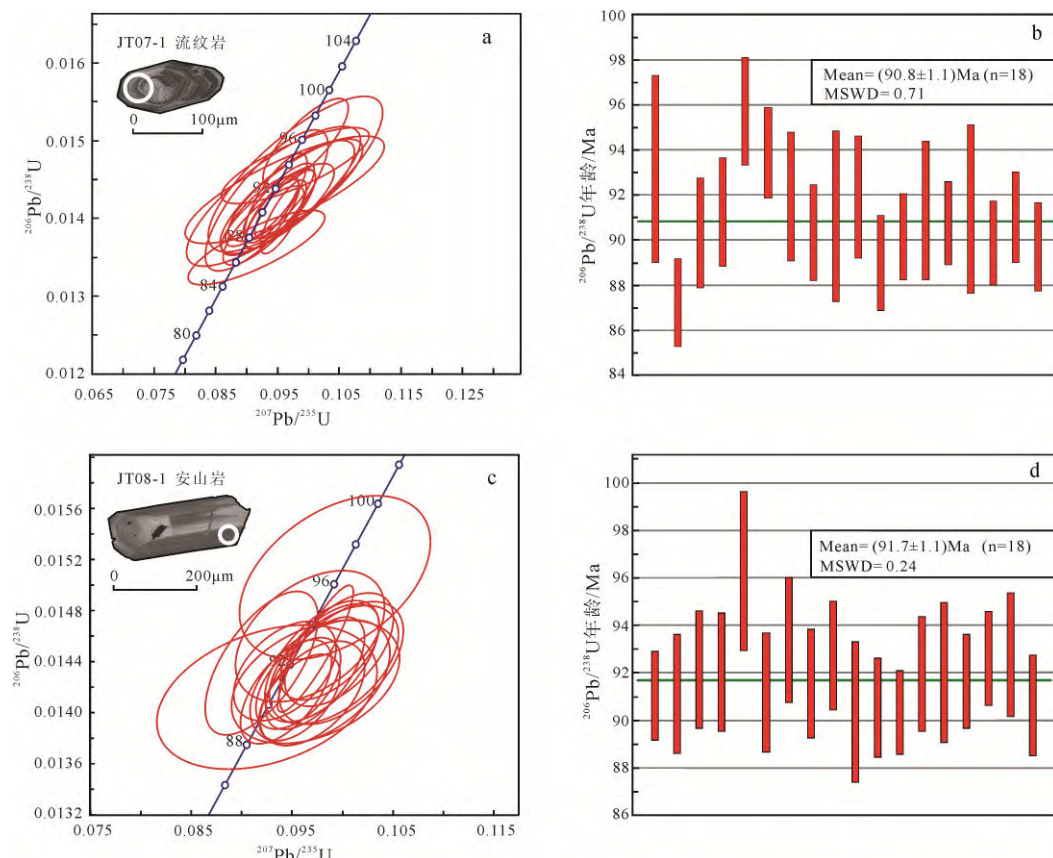
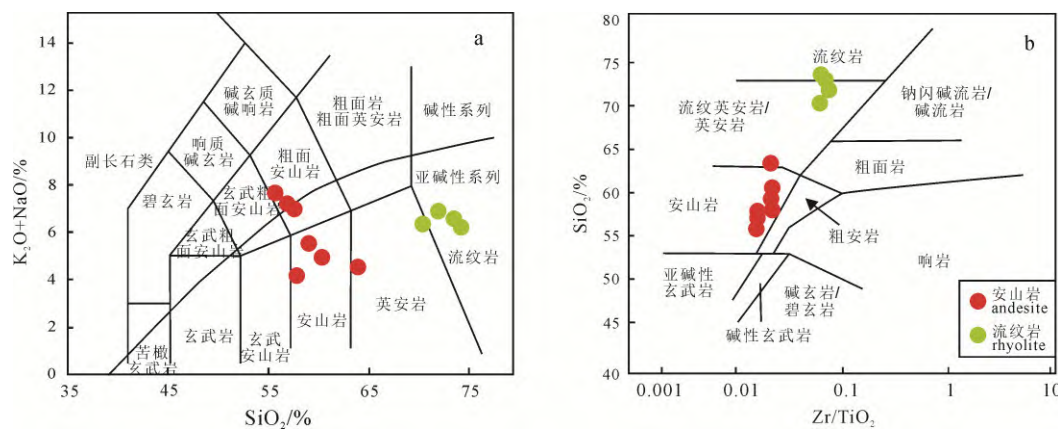


图 3 桑日地区晚白垩世火山岩 U-Pb 年龄谐和图(a, c)和加权平均年龄图(b, d)

Fig. 3 U-Pb age concordant diagram (a, c) and weighted mean age diagram (b, d) of Late Cretaceous volcanic rocks in the Sangri area

图 4 桑日地区晚白垩世火山岩(K<sub>2</sub>O+NaO)-SiO<sub>2</sub>(a)和SiO<sub>2</sub>-Zr/TiO<sub>2</sub>(b)图解

(a据 Frost et al., 2001; b据 Winchester and Floyd, 1977)

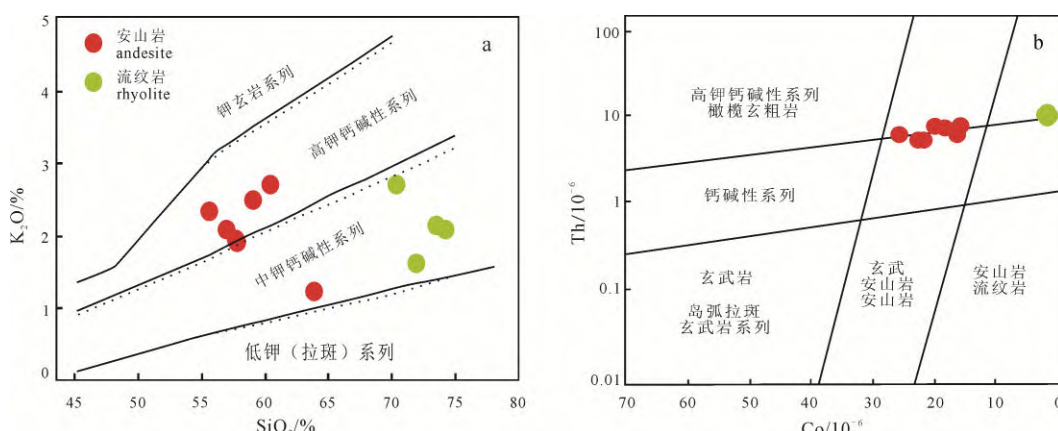
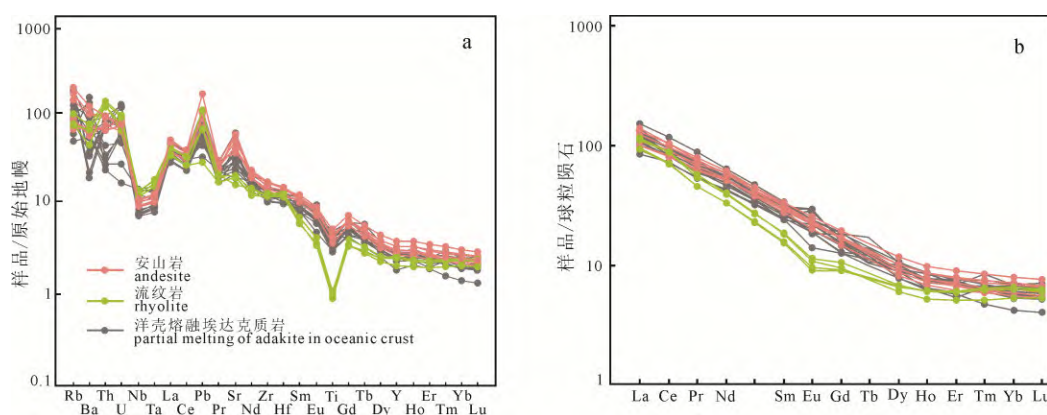
Fig. 4 (K<sub>2</sub>O+NaO)-SiO<sub>2</sub>(a) and SiO<sub>2</sub>-Zr/TiO<sub>2</sub>(b) diagrams for Late Cretaceous volcanic rocks in the Sangri area  
(a after Frost et al., 2001; b after Winchester and Floyd, 1977)图 5 桑日地区晚白垩世火山岩 K<sub>2</sub>O-SiO<sub>2</sub>(a) 和 Th-Co(b) 图解(a据 Rickwood, 1989; b据 Hastie et al., 2007)Fig. 5 K<sub>2</sub>O-SiO<sub>2</sub>(a) and Th-Co (b) diagrams for Late Cretaceous volcanic rocks in the Sangri area  
(a after Rickwood, 1989; b after Hastie et al., 2007)

图 6 桑日地区晚白垩世火山岩微量元素原始地幔标准化蛛网图(a)和稀土元素球粒陨石标准化分配模式图(b)(a, b 据 Sun and McDonough, 1989; 洋壳熔融埃达克质岩数据来自 Zhu et al., 2009; 代作文等, 2018; Zhang et al., 2018)

Fig. 6 Primitive mantle-normalized trace element diagram (a) and chondrite-normalized rare earth element (REE) diagram (b) for Late Cretaceous volcanic rocks in the Sangri area (a and b after Sun and McDonough, 1989; Data on adakite rocks were obtained from Zhu et al., 2009; DAI et al., 2018; Zhang et al., 2018)

量为 1.31%~1.65%(平均 1.52%), Mg<sup>#</sup>值为 52.96~55.72(平均 54.15), K<sub>2</sub>O 的含量为 1.65%~2.75%(平均 2.17%), Na<sub>2</sub>O 的含量为 3.71%~5.42%(平均 4.45%) 及较低的 K<sub>2</sub>O/Na<sub>2</sub>O 比值(平均为 0.51), 属于钙碱性岩石(图 5)。

### 3.2.2 微量、稀土元素

微量元素特征显示桑日地区晚白垩世安山岩样品相对富集 Rb、Sr、Pb 等大离子亲石元素和相对亏损 Nb、Ta、Ti 等高场强元素, 具有弧火山岩的特征(图 6a)。安山岩样品总稀土含量介于

表 1 桑日晚白垩世火山岩 Sr-Nd 同位素分析数据

Table 1 Sr-Nd isotope analysis data for Late Cretaceous volcanic rocks in the Sangri area

样品编号	JT07-1	JT07-2	JT08-1	JT08-2
岩性	流纹岩	流纹岩	安山岩	安山岩
$^{87}\text{Rb}/^{86}\text{Sr}$	0.341 560	0.325 160	0.207 010	0.182 760
$^{87}\text{Sr}/^{86}\text{Sr}$	0.704 948	0.704 734	0.704 418	0.704 426
$(^{87}\text{Sr}/^{86}\text{Sr})_i$	0.704 515	0.704 321	0.704 152	0.704 191
$^{147}\text{Sm}/^{144}\text{Nd}$	0.095 890	0.096 230	0.098 510	0.103 070
$^{143}\text{Nd}/^{144}\text{Nd}$	0.512 768	0.512 734	0.512 809	0.512 738
$(^{143}\text{Nd}/^{144}\text{Nd})_i$	0.512 711	0.512 677	0.512 750	0.512 676
$\varepsilon_{\text{Nd}}(t)$	3.700 000	3.000 000	4.500 000	3.000 000
$T_{\text{DM1}}/\text{Ma}$	497.000 000	543.000 000	454.000 000	571.000 000
$T_{\text{DM2}}/\text{Ma}$	590.000 000	645.000 000	527.000 000	646.000 000

122.91×10<sup>-6</sup>~151.82×10<sup>-6</sup> 之间, 平均值为 137.97×10<sup>-6</sup>。其中 Y 含量为 11.2×10<sup>-6</sup>~15.8×10<sup>-6</sup>, 平均 13.1×10<sup>-6</sup>, Yb 含量为 0.97×10<sup>-6</sup>~1.38×10<sup>-6</sup>, 平均 1.14×10<sup>-6</sup>, (La/Yb)<sub>N</sub>=14.04~24.08。如图 6b 所示, 轻重稀土分馏明显, 呈现有倾趋势, 显示轻稀土富集, 重稀土亏损的特点。 $\delta\text{Eu}=0.97\sim1.08$ , 平均值为 1, 钕异常不明显。

桑日流纹岩与安山岩具有相似的微量元素特征, 富集 Rb、Sr、Pb 等大离子亲石元素和相对亏损 Nb、Ta、Ti 等高场强元素, 具有弧火山岩特征(图 6a)。流纹岩样品总稀土含量介于 96.93×10<sup>-6</sup>~118.21×10<sup>-6</sup> 之间, 平均值为 107.58×10<sup>-6</sup>。其中 Y 含量为 8.36×10<sup>-6</sup>~10.9×10<sup>-6</sup>, 平均 10×10<sup>-6</sup>, Yb 含量为 0.92×10<sup>-6</sup>~1.11×10<sup>-6</sup>, 平均 1.04×10<sup>-6</sup>, (La/Yb)<sub>N</sub>=14.51~22.06。如图 6b 所示, 轻重稀土分馏明显, 呈现有倾趋势, 显示轻稀土富集, 重稀土亏损的特点。 $\delta\text{Eu}=0.74\sim0.81$ , 平均值为 0.78, 显示出微弱的铕异常, 这代表在岩石形成过程中斜长石分离结晶作用不明显。

### 3.2.3 Sr-Nd 同位素

本文挑选 4 件桑日地区晚白垩世火山岩样品(JT07-1、JT07-2、JT08-1 和 JT08-2)进行全岩 Sr-Nd 同位素分析。根据岩石锆石 U-Pb 定年结果, 分别计算初始 Sr 和 Nd 同位素比值, 分析结果见表 1。桑日地区晚白垩世火山岩的  $^{87}\text{Sr}/^{86}\text{Sr}$  初始值和  $^{143}\text{Nd}/^{144}\text{Nd}$  初始值变化范围较小, 分别为 0.704 152~0.704 515, 0.512 676~0.512 750。样品的  $\varepsilon_{\text{Nd}}(t)$  为正值, 在 3.0~4.5 之间, 二阶段模式年龄( $T_{\text{DM2}}$ )为 527~646 Ma。

## 4 讨论

### 4.1 桑日地区中生代火山岩的形成时代

拉萨地体南缘桑日地区中生代火山岩的形成时代一直是该区地质研究的重点。近年来, 前人在此开展了较多的年代学研究, 得到了多组火山岩锆石 U-Pb 年龄(图 1c), 初步构建了区域中生代火山岩

的年代学格架。Zhu et al.(2009)和康志强等(2015)对马门附近的麻木下组火山岩进行了年代学研究, 得到其锆石 U-Pb 年龄为 136~100 Ma, 属于早白垩世; 康志强等(2015)和 Ran et al.(2019)在旦师庭庙附近获得了晚白垩世旦师庭组火山岩的锆石 U-Pb 年龄(97~90 Ma), 表明其形成于晚白垩世。而前人在不同地区获得的比马组火山岩年代学数据差别较大, 早期依据六射珊瑚、圆粒虫、腹足及双壳类等生物化石, 将比马组的形成时代划归至早白垩世(西藏自治区地质调查院, 2003); 1: 20 万泽当幅区域地质调查报告中比马组安山岩 Rb-Sr 等时线年龄为白垩纪(125.23~92.76 Ma)。近年来随着地质工作程度的不断加深, 比马组的形成时代甚至可以追溯至早侏罗世。Kang et al.(2014)报道了桑日地区卡马档比马组火山岩锆石 U-Pb 年龄为 195~189 Ma, 表明形成于早侏罗世; Ma et al.(2017)在荣玛乡比马组安山岩中获得了中侏罗世的年龄数据(170.2~165.1 Ma); Chen et al.(2019)在南木林桑宗比马组安山岩中获得了中侏罗世的年龄数据((167.8±2.5) Ma); Lang et al.(2020)在谢通门县达那答乡比马组火山岩中获得了中侏罗世的年龄数据(184.3~176.8 Ma); 闫国强等(2014)在山南努日矿区比马组安山岩中获得了晚白垩世的锆石 U-Pb 年龄((92.04±0.71) Ma)。

比马组火山岩主要出露在桑日、乃东、加查地区, 地层厚度较大且沉积夹层较多, 西部尼木、南木林一带亦有零星出露, 多呈残体出现, 其厚度较小, 沉积夹层相对较少, 典型剖面位于桑日县西侧, 主体为中性火山岩, 夹中酸性火山岩、结晶灰岩、砂岩、粉砂岩, 区域厚度变化较大, 但延伸稳定(康志强等, 2010; 黄丰等, 2015; 杨宗耀等, 2019)。本次研究选择桑日县西侧塔木村附近的比马组火山岩进行锆石 U-Pb 定年, 结果显示其年龄为 92~91 Ma, 结合比马组整合接触于麻木下组之上的野外事实, 本文获得的锆石 U-Pb 年龄是合理的。作者认为造成不同地区比马组年代学数据差别的原因有以下两

点：(1)拉萨地体南缘自中生代以来，先后经历了新特提斯洋俯冲消减、消亡及印亚大陆碰撞的演化过程(Yin and Harrison, 2000; 潘桂棠等, 2006; 许志琴等, 2011; Zhu et al., 2011, 2013)，岩浆作用频繁，具有多期次演化的特点，容易造成不同地区比马组火山岩年龄的差异；(2)比马组火山岩在演化后期容易被冈底斯岩基所侵吞，对于其火山沉积序列和接触关系不明确，加上当时技术条件的限制，缺少精确的年代学数据，因此早期根据沉积序列和岩性组合划分的地层单位可能包含了不同时代的火山岩。综合上述比马组火山岩的锆石 U-Pb 年龄数据，表明不同地区比马组火山岩的形成时代跨度较大，可能受到多期岩浆作用影响，因此，对于不同地段的比马组火山岩的时代归属问题还需要进一步细化研究，本文锆石 U-Pb 定年结果为比马组火山岩的年代学研究提供了新的资料。

#### 4.2 桑日地区晚白垩世火山岩的构造环境

本文样品 LOI 在 1.35~4.36 之间，镜下又观察到岩石遭受到蚀变，因此在分析样品构造环境和成因之前，需要对所用元素的稳定性进行投图分析。 $Zr$  在岩浆演化过程中能稳定存在，通常用它来衡量其它元素的稳定性(Wood, 1979)。如图 7 所示，主量、微量元素和稀土元素均与  $Zr$  显示出良好的相关性，表明岩石未经历较强的蚀变。

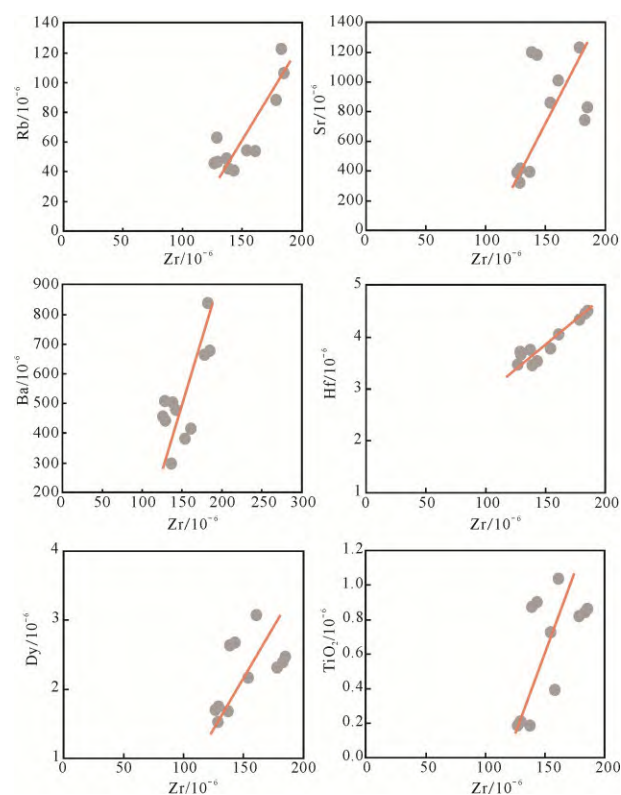


图 7 桑日地区晚白垩世火山岩元素-Zr 图解  
(据 Bao et al., 2004)

Fig. 7 Element-Zr diagram of Late Cretaceous volcanic rocks in the Sangri area (after Bao et al., 2004)

拉萨地体南缘中生代岩浆作用与新特提斯洋的演化密切相关，受新特提斯洋北向俯冲的影响，分布在拉萨地体南缘的火山岩大多具有弧岩浆岩的特征(吴旌等, 2014)。桑日地区晚白垩世火山岩属于钙碱性系列，具有较高的  $Al_2O_3$  含量和  $Na_2O/K_2O$  比值(表 2)，富集大离子亲石元素(Rb、Sr 和 Pb)和轻稀土元素，亏损高场强元素(Nb、Ta 和 Ti)和重稀土元素，反映出火山岩样品形成于俯冲带环境，具有弧岩浆岩的特征。图 Th/Ta-Yb 和 Th-Ta(图 8)可用来区分形成于不同构造环境下的弧火山岩，桑日地区晚白垩世火山岩样品全部落入活动大陆边缘，表明其形成于活动大陆边缘；在图 9 中，样品全部落入火山弧花岗岩区域中，进一步验证和约束了火山岩的构造环境。综合岩石地球化学特征和构造环境判别图解，认为桑日地区晚白垩世火山岩形成于活动大陆边缘环境。

白垩纪时期，拉萨地体南部有新特提斯洋，北部有班公湖-怒江洋。桑日地区晚白垩世火山岩的形成与哪一个大洋的俯冲有关呢？从时间上看，众多学者虽然对班公湖-怒江洋的最终闭合时间存有较大争议，闭合时间从晚侏罗至晚白垩世均有(Yin and Harrison, 2000; Kapp et al., 2003; Hao et al., 2015; 方向等, 2015; 高腾等, 2019)，李华亮等(2016)报道的

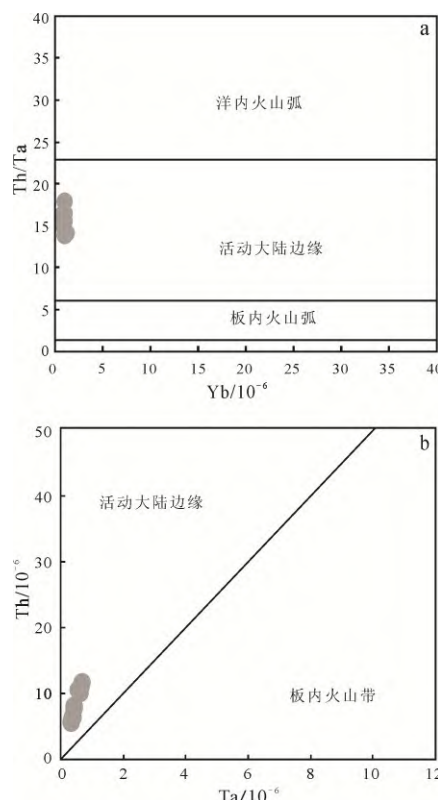


图 8 桑日地区晚白垩世火山岩 Th/Ta-Yb(a)和 Th-Ta(b)图解(a 据 Gorton and Schandl, 2000;  
b 据宋志伟等, 2021)

Fig. 8 Th/Ta-Yb (a) and Th-Ta (b) diagrams of Late Cretaceous volcanic rocks in the Sangri area (a after Gorton and Schandl, 2000; b after SONG et al., 2021)

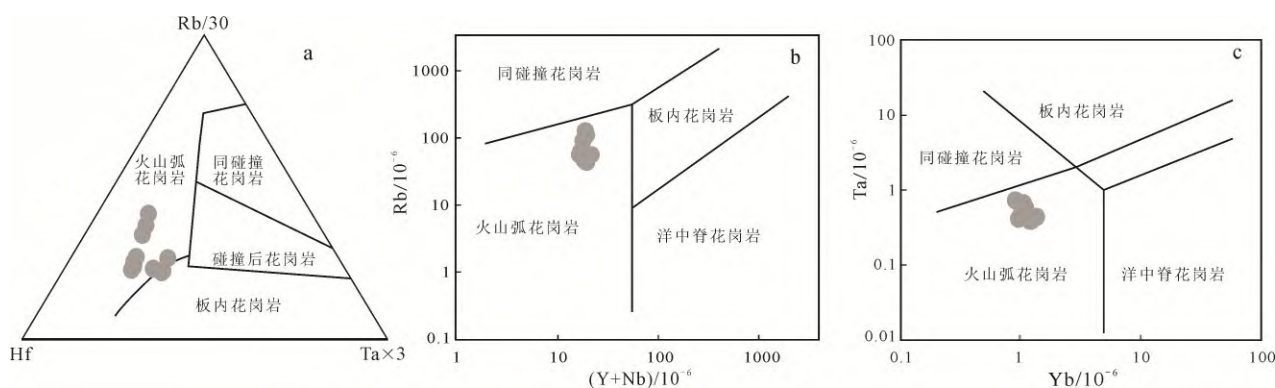


图 9 桑日地区晚白垩世火山岩 Rb/30-Hf-Tax3、Rb-(Y+Nb)(b) 和 Ta-Yb(c) 图解

(a 据 Harris et al., 1986; b, c 据 Pearce et al., 1984)

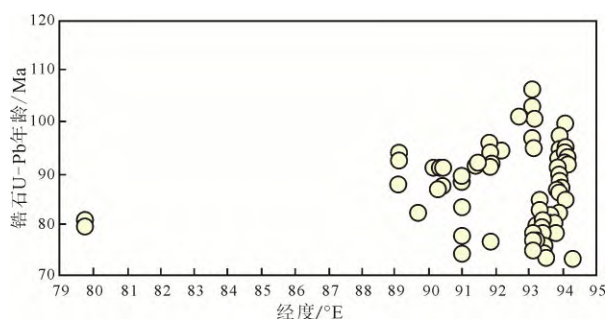
Fig. 9 Rb/30-Hf-Tax3, Rb-(Y+Nb) (b) and Ta-Yb (c) diagrams of Late Cretaceous volcanic rocks in the Sangri area  
(a after Harris et al., 1986; b and c after Pearce et al., 1984)

图 10 拉萨地体南缘晚白垩世锆石 U-Pb 年龄经度分布图(据 Zhu et al., 2018)

Fig. 10 Zircon U-Pb age-longitude of the Late Cretaceous rocks on the southern margin of Lhasa terrane  
(after Zhu et al., 2018)

晚白垩世沉积的竟柱山组(96 Ma)可以认为是班公湖-怒江洋闭合的最晚期限。从距离上来看, 桑日地区晚白垩世火山岩位于拉萨地体南缘, 距离班公湖-怒江洋超过 300 km, 如果考虑到拉萨地块在白垩纪到古近纪发生了大量地壳加厚缩短的地质事件(England and Houseman, 1986; 潘桂棠等, 2004), 桑日地区晚白垩世火山岩出露的位置可能距离班公湖-怒江洋超过 500 km。另外, 基于岩浆岩、沉积岩综合研究结果显示, 班公湖-怒江洋壳仅向北俯冲到羌塘地体之下(Hao et al., 2015; Huang et al., 2016), 因此桑日地区晚白垩世火山岩不太可能受到班公湖-怒江洋南向俯冲的影响。

基于前人研究, 米林-朗县一带、桑日-扎囊一带和曲水-尼木-日喀则一带先后多次报道了晚白垩世岩浆作用, 其年龄主要集中在 100~80 Ma, 岩石类型复杂多样(Ma et al., 2013b; 叶丽娟等, 2015; 王珍珍等, 2017; 代作文等, 2018)。据已有的区域地质调查资料和年代学数据(Zhu et al., 2018), 拉萨地体南缘的晚白垩世时期(100–80 Ma)岩浆作用活跃(图 10), 爆发了较大规模的平行于雅鲁藏布江缝合带走向的岩浆活动(图 1b), 与新特提斯洋的

北向俯冲有关(王金丽等, 2009; Zhang et al., 2010; Ma et al., 2013a)。本文得到的桑日火山岩的锆石 U-Pb 年龄为 92~91 Ma, 与上述晚白垩世岩浆作用时代一致, 很有可能与这一时期爆发的岩浆是同一阶段、同一构造环境的产物。因此, 以上特征表明桑日地区晚白垩世火山岩形成于新特提斯洋北向俯冲消减有关的活动大陆边缘。

### 4.3 岩石成因

桑日地区晚白垩世火山岩样品 Y( $8.36 \times 10^{-6}$ ~ $15.8 \times 10^{-6}$ )、Yb( $0.92 \times 10^{-6}$ ~ $1.38 \times 10^{-6}$ )含量较低, Sr/Y 比值(36.28~105.59)较高, 除 JT07-1、JT07-3 和 JT07-4 的 Sr 含量小于  $400 \times 10^{-6}$  外, 其余均高于  $400 \times 10^{-6}$ , 全部样品 Sr 的平均含量为  $779 \times 10^{-6}$ , 火山岩样品的地球化学性质基本与埃达克岩相符。在 Sr/Y-Y 和 (La/Yb)<sub>N</sub>-Yb<sub>N</sub> 的图解中(图 11), 几乎全部桑日地区晚白垩世火山岩样品都落在埃达克岩区域, 表明其属于埃达克质岩。

典型的埃达克岩起源于年轻的、热的俯冲洋壳的部分熔融(Defant and Drummond, 1990; Kay and Kay, 1993; Stern and Kilian, 1996)。随后, 越来越多的研究证明, 具有与埃达克岩相似属性的岩石不仅可以在岛弧环境下出现, 在陆-陆碰撞造山带和板内伸展等构造环境中均有埃达克岩的存在(王强等, 2008)。关于埃达克质岩的成因, 不同学者提出了不同的形成模式: (1)增厚镁铁质的下地壳熔融(Wen et al., 2008a; 管琪等, 2010); (2)玄武质岩浆的分异结晶作用(Macpherson et al., 2006); (3)玄武质岩浆和长英质岩浆的混合作用(Streck et al., 2007); (4)俯冲洋壳的部分熔融(Zhu et al., 2009; Zhang et al., 2010; Zheng et al., 2014; Chen et al., 2015; Wang et al., 2019)。鉴于以上多种成因, 下面将逐一讨论最有可能的成岩方式。

起源于增厚镁铁质下地壳部分熔融的埃达克

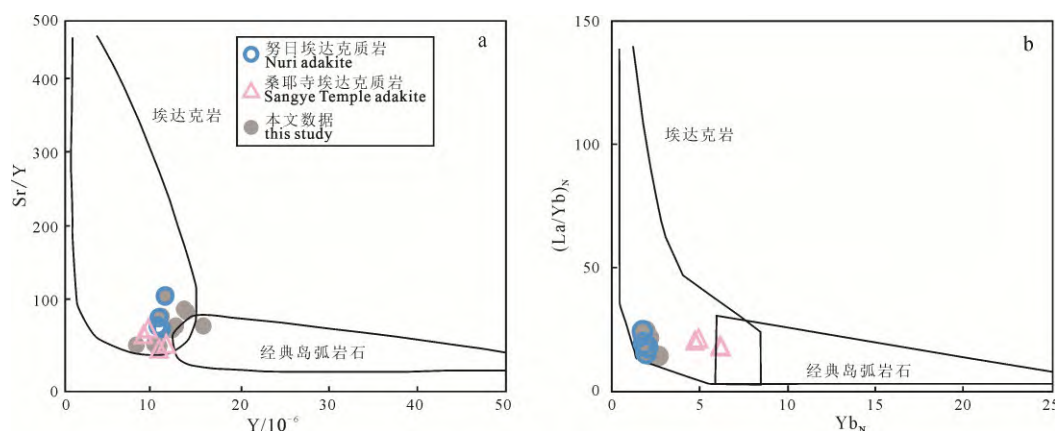


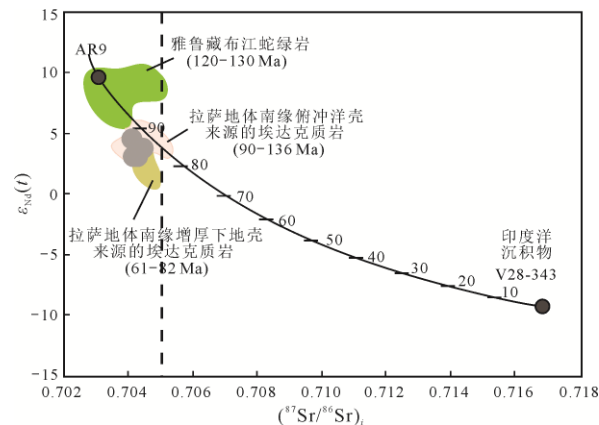
图 11 桑日地区晚白垩世火山岩 Sr/Y-Y 判别图(a)和(La/Yb)<sub>N</sub>-Yb<sub>N</sub> 判别图(b)

(a 据 Defant and Drummond, 1990; b 据 Martin et al., 2005)

Fig. 11 Sr/Y-Y discrimination diagram (a) and (La/Yb)<sub>N</sub>-Yb<sub>N</sub> discrimination diagram (b) of Late Cretaceous volcanic rocks in the Sangri area (a, according to Defant and Drummond, 1990; b, according to Martin et al., 2005)

质岩通常具有低 MgO 含量和 Mg<sup>#</sup>值(Smithies, 2000; Prouteau et al., 2001)。如拉萨地体南缘米林地区报道的起源于下地壳部分熔融的晚白垩世埃达克质岩, 其 Mg<sup>#</sup>值介于 33~40 之间(管琪等, 2010)。桑日地区晚白垩世火山岩具有较高的 Mg<sup>#</sup>, 全部样品的 Mg<sup>#</sup>均大于 40, 同时还具有较高的 Cr 和 Ni 含量, 这些特征均不同于加厚下地壳熔融形成的埃达克岩。此外, 有研究表明, 镁铁质岩石在超过地下 40 km 的深度才有可能形成埃达克质岩(Sen and Dunn, 1994; Rapp and Watson, 1995)。目前拉萨地块地壳的平均厚度在 50~70 km, 然而对于其隆升历史有不同看法。一部分学者认为, 拉萨地块地壳于 80 Ma 左右明显加厚(张泽明等, 2019; Tang et al., 2020)。而另一部分学者认为在 70 Ma 之前, 拉萨地块地壳可能是正常厚度, 大约为 37 km。55~45 Ma 时, 西藏地壳由于板块断裂、碰撞等原因导致隆升, 才广泛达到现在的高度(Zhu et al., 2017)。由此看来, 南部拉萨地体地壳是否在 90 Ma 加厚到 40 km 具有较大争议。同时, 在桑日地区晚白垩世火山岩  $\varepsilon_{\text{Nd}}(t)$ -(<sup>87</sup>Sr/<sup>86</sup>Sr)<sub>i</sub> 图解中(图 12)可以看出, 研究样品并未落入拉萨地体南缘增厚下地壳来源的埃达克质岩区域中, 表明桑日地区晚白垩世火山岩不太可能通过增厚下地壳熔融产生。

另外, 桑日地区晚白垩世火山岩也不太可能是由玄武质岩浆分异结晶而成: (1)本文研究的样品主要由中性岩、酸性岩构成, 研究区附近没有发现同时期的基性岩。同时作者综合拉萨地体南缘晚白垩世岩浆作用的数据发现区域上也鲜有基性岩的报道(图 13), 缺少大面积出露基性岩的证据; (2)如图 14 所示, 桑日地区晚白垩世火山岩样品点总体呈现出较为清晰的正相关性, 指示岩浆活动以部分熔融作用为主; (3)玄武质岩浆分异过程中, 高压条件下的结晶分异作用会导致 Dy/Yb 比值随分异结晶作用而



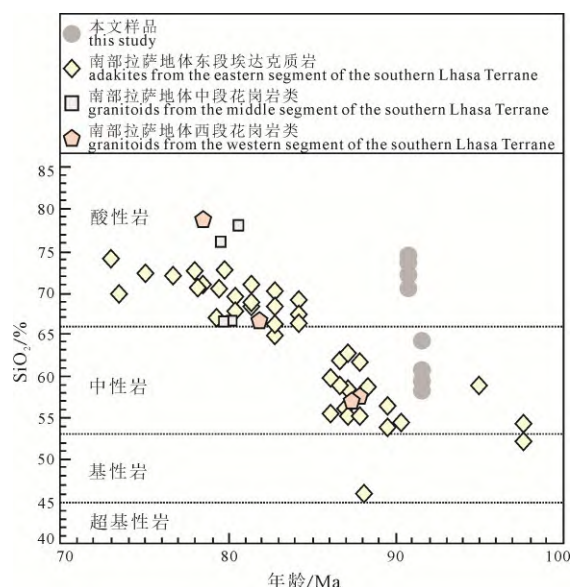
数据来源: 雅鲁藏布江蛇绿岩数据来源于 Xu and Castillo, 2004; Zhang et al., 2005; 牛晓露等, 2006; 拉萨地体南缘俯冲洋壳来源的埃达克质岩数据来源于 Zhu et al., 2009; Jiang et al., 2012, 2014; 拉萨地体南缘增厚下地壳来源的埃达克质岩数据来源于 Wen et al., 2008b; Jiang et al., 2014; AR9 据牛晓露等, 2006 ( $\text{Sr}=131 \times 10^{-6}$ , (<sup>87</sup>Sr/<sup>86</sup>Sr)<sub>i</sub>=0.703 309, Nd=9.46×10<sup>-6</sup>,  $\varepsilon_{\text{Nd}}(t)=+9.6$ ); 印度洋沉积物据 Othman et al., 1989; V28-343( $\text{Sr}=119 \times 10^{-6}$ , (<sup>87</sup>Sr/<sup>86</sup>Sr)<sub>i</sub>=0.716 82, Nd=23.05×10<sup>-6</sup>,  $\varepsilon_{\text{Nd}}(t)=-9.3$ )。

Data sources: Ophiolites from Yarlung Zangbo River were obtained from Xu and Castillo, 2004; Zhang et al., 2005; NIU et al., 2006; data on adakites derived from subduction oceanic crust in the southern margin of Lhasa terrane were obtained from Zhu et al., 2009; Jiang et al., 2012, 2014; adakite data from the thickened lower crust of the southern margin of Lhasa terrane were obtained from Wen et al., 2008b; Jiang et al., 2014; AR9 according to NIU et al., 2006 ( $\text{Sr}=131 \times 10^{-6}$ , (<sup>87</sup>Sr/<sup>86</sup>Sr)<sub>i</sub>=0.703 309, Nd=9.46×10<sup>-6</sup>,  $\varepsilon_{\text{Nd}}(t)=+9.6$ ); Indian Ocean sediments according to Othman et al., 1989; V28-343 ( $\text{Sr}=119 \times 10^{-6}$ , (<sup>87</sup>Sr/<sup>86</sup>Sr)<sub>i</sub>=0.716 82, Nd=23.05×10<sup>-6</sup>,  $\varepsilon_{\text{Nd}}(t)=-9.3$ ).

图 12 桑日地区晚白垩世火山岩  $\varepsilon_{\text{Nd}}(t)$ -(<sup>87</sup>Sr/<sup>86</sup>Sr)<sub>i</sub> 图解

Fig. 12  $\varepsilon_{\text{Nd}}(t)$ -(<sup>87</sup>Sr/<sup>86</sup>Sr)<sub>i</sub> diagram of Late Cretaceous volcanic rocks in the Sangri area

显著增大(Wang et al., 2019)。在 Sr/Y-SiO<sub>2</sub> 和 Dy/Yb-SiO<sub>2</sub> 图解中(图 15a, b), 桑日地区晚白垩世火山岩样品的 Sr/Y 和 Dy/Yb 比值并没有随着 SiO<sub>2</sub> 含量的增大而增大, 进一步说明桑日地区晚白垩世火山岩不可能由玄武质岩浆高压分异结晶形成。玄武质岩浆的低压分异结晶作用通常会涉及斜长石从



数据来源: 南部拉萨地体东段埃达克质岩数据来自 Wen et al., 2008a; 管琪等, 2010, 2011; Zhang et al., 2010; 南部拉萨地体中段花岗岩类数据来自黄玉等, 2010; Zhu et al., 2011; 南部拉萨地

体西段花岗岩类数据来自 Zhu et al., 2011。

Data source: daktite rocks in the eastern part of Southern Lhasa were obtained from Wen et al., 2008a; GUAN et al., 2010, 2011; Zhang et al., 2010; data on granitoids in the middle part of the Southern Lhasa terrane were obtained from HUANG et al., 2010; Zhu et al., 2011; data on granitoids in the western segment of the Southern Lhasa terrane were obtained from Zhu et al., 2011.

图 13  $\text{SiO}_2$ -年龄(Ma)图解(据管琪等, 2011)

Fig. 13  $\text{SiO}_2$ -age (Ma) diagram (after GUAN et al., 2011)

母岩浆的分离, 斜长石的分异结晶作用会造成  $\text{Zr}/\text{Sm}$  比值的升高和 Eu 的负异常。在稀土元素配分模式图上桑日地区晚白垩世火山岩未见明显 Eu 的

负异常(图 6b)。在  $\delta\text{Eu}-\text{SiO}_2$  和  $\text{Zr}/\text{Sm}-\text{SiO}_2$  图解上(图 15c, d), 未见  $\delta\text{Eu}$  和  $\text{Zr}/\text{Sm}$  值与  $\text{SiO}_2$  呈现相关关系, 说明岩浆并未发生斜长石的分离结晶。由此看来, 桑日地区晚白垩世火山岩不是由玄武质岩浆低压分异结晶作用形成的。综上所述, 可以排除桑日地区晚白垩世火山岩是由玄武质岩浆分异结晶作用形成。

埃达克质岩可以由玄武质和长英质岩浆混合而成, 我国东北部古新世的埃达克质岩的成因就是岩浆混合(Qin et al., 2007)。桑日地区晚白垩世火山岩显示出较均一的 Sr-Nd 同位素成分 ( $(^{87}\text{Sr}/^{86}\text{Sr})=0.704~152\sim0.704~515$ ,  $\varepsilon_{\text{Nd}}(t)=3.0\sim4.5$ ), 不支持研究样品是由玄武质和长英质岩浆混合而成。同时岩浆混合成因的埃达克质岩通常具有相对较高的  $\text{MgO}$  含量和  $\text{Mg}^{\#}$  值( $\text{MgO}>4.5\%$ ,  $\text{Mg}^{\#}>66$ ; 李晓寒, 2015)。桑日地区晚白垩世火山岩的  $\text{MgO}$  含量和  $\text{Mg}^{\#}$  与之相比较低, 这表明其不是岩浆混合作用形成的。此外, 在野外调查过程中未发现有反映混合作用的暗色铁镁质包体, 进一步说明桑日地区晚白垩世火山岩不是岩浆混合作用的产物。

因此, 桑日地区晚白垩世火山岩最可能是由俯冲洋壳的部分熔融形成的: (1)如图 6a 所示, 研究样品的微量元素地球化学特征显示, 其富集大离子亲石元素 Rb、Sr 和 Pb, 亏损高场强元素 Nb、Ta 和 Ti, 与区域上前人报道的同时期马门埃达克质岩、努日埃达克质岩和桑耶寺埃达克质岩稀土微量元素

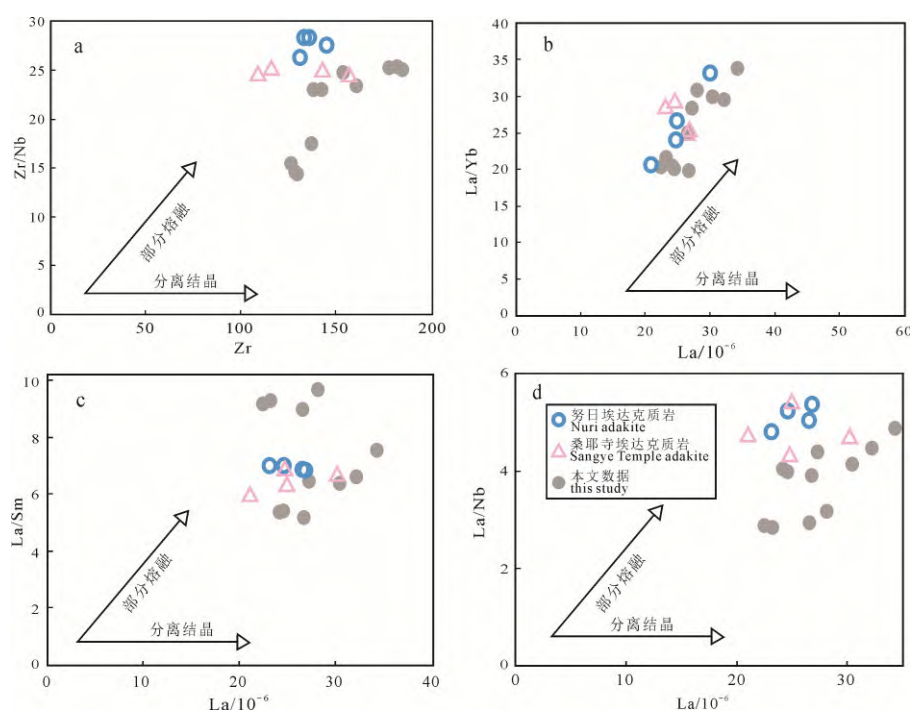
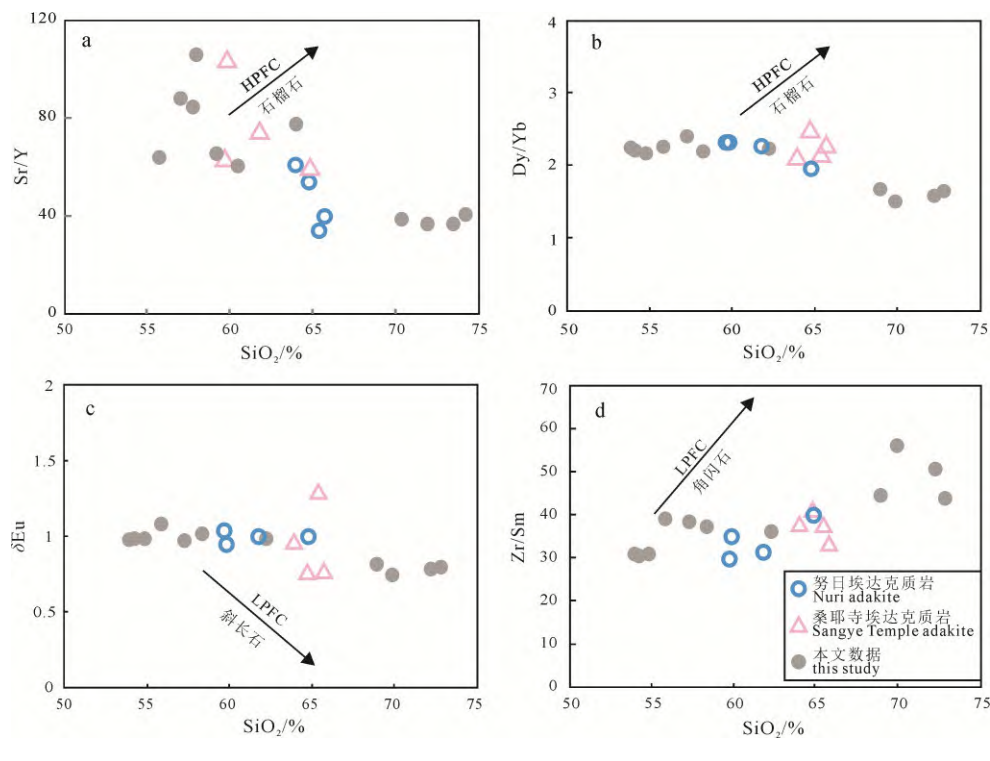


图 14 桑日地区晚白垩世火山岩  $\text{Zr}/\text{Nb}-\text{Zr}$ (a)、 $\text{La}/\text{Yb}-\text{La}$ (b)、 $\text{La}/\text{Sm}-\text{La}$ (c) 和  $\text{La}/\text{Nb}-\text{La}$ (d) 图解

(a 据 Geng et al., 2009; b 据 Chung et al., 2009; c 据 Wang et al., 2019)

Fig. 14  $\text{Zr}/\text{Nb}-\text{Zr}$  (a),  $\text{La}/\text{Yb}-\text{La}$  (b),  $\text{La}/\text{Sm}-\text{La}$  (c), and  $\text{La}/\text{Nb}-\text{La}$  (d) diagrams of Late Cretaceous volcanic rocks in the Sangri area (a after Geng et al., 2009; b after Chung et al., 2009; c after Wang et al., 2019)

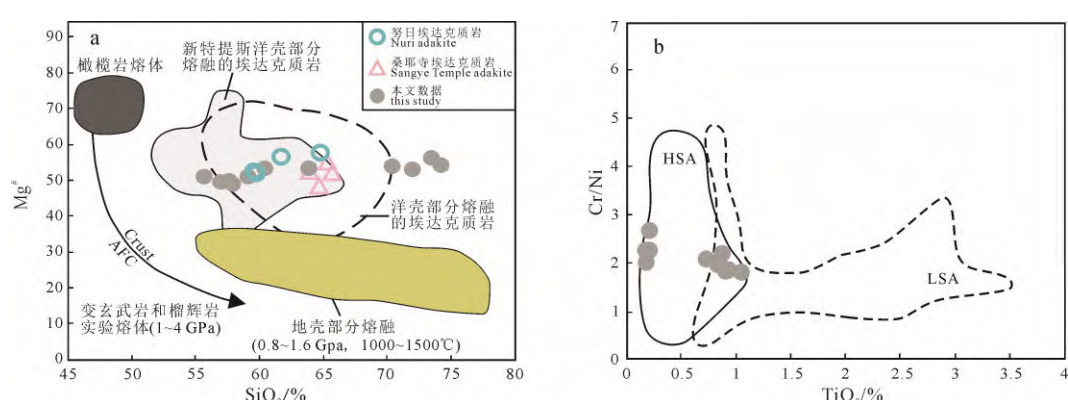


HPFC—高压分异结晶作用; LPFC—低压分异结晶作用。

HPFC—high pressure fractional crystallization; LPFC—low pressure fractional crystallization.

图 15 桑日地区晚白垩世火山岩  $\text{Sr}/\text{Y}$ - $\text{SiO}_2$ (a)、 $\text{Dy}/\text{Yb}$ - $\text{SiO}_2$ (b)、 $\delta\text{Eu}$ - $\text{SiO}_2$ (c)和  $\text{Zr}/\text{Sm}$ - $\text{SiO}_2$ (d)图解

Fig. 15  $\text{Sr}/\text{Y}$ - $\text{SiO}_2$  (a),  $\text{Dy}/\text{Yb}$ - $\text{SiO}_2$  (b),  $\delta\text{Eu}$ - $\text{SiO}_2$  (c) and  $\text{Zr}/\text{Sm}$ - $\text{SiO}_2$  (d) diagrams of Late Cretaceous volcanic rocks in the Sangri area (a, b, c after Wang et al., 2019; d after Drummond et al., 1996)



数据来源: 起源于洋壳部分熔融的埃达克质岩石据 Wang et al., 2006; 下地壳部分熔融据 Rapp and Watson, 1995;

起源于新特提斯洋壳部分熔融的埃达克质岩石区域据 Zhu et al., 2009; Jiang et al., 2012; Ma et al., 2013b。

Data source: adakite rocks were obtained from partial melting of oceanic crust, Wang et al., 2006; partial melting of the lower crust after Rapp and Watson, 1995; adakite rocks were obtained from the partial melting of the NeoTethyan ocean crust after Zhu et al., 2009; Jiang et al., 2012; Ma et al., 2013b.

图 16 桑日地区晚白垩世火山岩  $\text{Mg}^{\#}$ - $\text{SiO}_2$ (a)和  $\text{Cr}/\text{Ni}$ - $\text{TiO}_2$ (b)图解(b 据吴昌坦, 2019)

Fig. 16  $\text{Mg}^{\#}$ - $\text{SiO}_2$  and  $\text{Cr}/\text{Ni}$ - $\text{TiO}_2$  diagram of Late Cretaceous volcanic rocks in the Sangri area (b after WU, 2019)

分布特征比较一致(如图 5), 暗示了二者之间具有成因上的联系。(2)张旗等(2001)将埃达克岩分为 O 型和 C 型两类: O 型埃达克岩富钠, 通常被解释为与俯冲洋壳的部分熔融有关; C 型埃达克岩富钾, 通常被解释为与加厚下地壳的部分熔融有关。桑日地区晚白垩世火山岩  $\text{NaO}/\text{K}_2\text{O}=1.20\sim 3.29$ (除一个样品为 0.84), 具有富钠的特点, 同时具有弧火山岩的特征, 说明了桑日地区晚白垩世火山岩属于 O 型

埃达克岩, 表明其成因与新特提斯洋壳的部分熔融有关。(3)在  $\text{Sr-Nd}$  同位素特征图上(图 12), 研究样品全部落入拉萨地体南缘俯冲洋壳来源的埃达克质岩区域内; 在  $\text{Mg}^{\#}$ - $\text{SiO}_2$  图解中(图 16a), 大部分桑日地区晚白垩世火山岩样品都投图在洋壳部分熔融成因的埃达克岩范围内。因此, 以上特征指示桑日地区晚白垩世火山岩可能起源于新特提斯洋壳的部分熔融。(4)Martin et al.(2005)研究表明, 洋壳熔体在

上升的过程中伴有地幔楔物质的加入形成高硅埃达克质岩(HSA), 低硅埃达克质岩(LSA)主要来源于长英质熔体交代地幔楔的部分熔融。如图 16b 所示, 该火山岩样品落在高硅埃达克岩区域内, 证明桑日地区晚白垩世火山岩起源于新特提斯洋壳的部分熔融, 同时可能伴有地幔楔物质的加入。实验岩石学发现, 在玄武质熔体中加入 10% 的橄榄岩可以使  $Mg^{\#}$  值从 44 上升到 55(Rapp et al., 1999)。桑日地区晚白垩世火山岩样品的  $Mg^{\#}$  值为 48.60~55.72, 暗示只有少量地幔楔物质的加入。

桑日地区晚白垩世火山岩具有一致的成岩年龄, 安山岩的年龄略早于流纹岩, 二者均富集大离子亲石元素和亏损高场强元素, 具有相似的地球化学特征(图 5a), 表明不同岩性的火山岩存在着密切的成因关系, 可能来自于同一源区。如图 13 所示, 桑日地区晚白垩世火山岩整体呈现部分熔融的趋势, 同时经历了相对较弱程度的分离结晶作用。火山岩演化过程中, 新特提斯洋壳熔体上升过程中伴有少量地幔楔物质的加入, 导致  $Mg^{\#}$  值、Cr 和 Ni 的含量升高, 形成了安山质的岩浆。与安山岩相比, 流纹岩形成时间略晚, 明显富硅, Cr、Ni 元素含量和稀土元素总量偏低, Eu 负异常偏强(附表 2), 暗示流纹岩可能是经过分离结晶作用演化的岩浆作用形成(张玉涛等, 2007)。综上分析, 桑日地区晚白垩世安山岩和流纹岩的母岩浆起源于新特提斯洋壳熔体, 熔体上升过程中伴有地幔楔物质的加入并经历了分离结晶作用。

## 5 结论

(1)本文报道的拉萨地体南缘桑日县西侧塔木村比马组火山岩年龄在 92~90 Ma 之间, 时代为晚白垩世。结合区域上定年结果表明比马组火山岩形成时代跨度大, 因此, 对于不同地段的比马组火山岩的时代归属问题需要进一步细化研究。

(2)桑日地区晚白垩世火山岩形成于新特提斯洋壳北向俯冲消减有关的活动大陆边缘。

(3)岩石地球化学特征显示本文研究的桑日地区晚白垩世火山岩是埃达克质岩, 安山岩和流纹岩的母岩浆起源于新特提斯洋壳的部分熔融, 熔体上升过程中伴有地幔楔物质的加入并经历了分离结晶作用。

## Acknowledgements:

This study was supported by Science and Technology Plan Project of Sichuan Province (No. 2020JDJQ0042), National Natural Science Foundation of China (Nos. 41502079 and 41972084), National Key Research and Development Program of China

(No. 2018YFC0604105), Chengdu University of Technology (No. 2020ZF11047), Northwest University (No. 18LCD04), Ministry of Natural Resources (No. ZS1911), and China Geological Survey (Nos. DD20190167 and DD20160346).

本文附有增强材料(附表 1, 2), 请通过本文网络版阅读或下载。

## 参考文献:

- 代作文, 李光明, 丁俊, 黄勇, 曹华文. 2018. 西藏努日晚白垩世埃达克岩: 洋脊俯冲的产物[J]. 地球科学, 43(8): 2727-2741.
- 方向, 唐菊兴, 宋杨, 杨超, 丁帅, 王艺云, 王勤, 孙兴国, 李玉彬, 卫鲁杰, 张志, 杨欢欢, 高轲, 唐攀. 2015. 西藏铁格隆南超大型浅成低温热液铜(金、银)矿床的形成时代及其地质意义[J]. 地球学报, 36(2): 168-176.
- 高腾, 王立强, 王勇, 郑斯伦, 胡宇. 2019. 班—怒成矿带西段江玛南铜银矿区石英闪长玢岩锆石 U-Pb 年龄、Hf 同位素及地球化学特征[J]. 地球学报, 40(6): 884-894.
- 管琪, 朱弟成, 赵志丹, 张亮亮, 刘敏, 李小伟, 于枫, 莫宣学. 2010. 西藏南部冈底斯带东段晚白垩世埃达克岩: 新特提斯洋脊俯冲的产物[J]. 岩石学报, 26(7): 2165-2179.
- 管琪, 朱弟成, 赵志丹, 董国臣, 莫宣学, 刘勇胜, 胡兆初, 袁洪林. 2011. 西藏拉萨地块南缘晚白垩世镁铁质岩浆作用的年代学、地球化学及意义[J]. 岩石学报, 27(7): 2083-2094.
- 侯增谦, 莫宣学, 高永丰, 杨志明, 董国臣, 丁林. 2006. 印度大陆与亚洲大陆早期碰撞过程与动力学模型——来自西藏冈底斯新生代火成岩证据[J]. 地质学报, 80(9): 1233-1248.
- 黄丰, 许继峰, 陈建林, 康志强, 董彦辉. 2015. 早侏罗世叶巴组与桑日群火山岩: 特提斯洋脊俯冲过程中的陆缘弧与洋内弧[J]. 岩石学报, 31(7): 2089-2100.
- 黄玉, 赵志丹, 张凤琴, 朱弟成, 董国臣, 周肃, 莫宣学. 2010. 西藏冈底斯仁布-拉萨一带花岗岩基的地球化学及其意义[J]. 岩石学报, 26(10): 3131-3142.
- 康志强, 付文春, 田光昊. 2015. 西藏桑日县地区中生代火山岩地层层序——基于锆石 U-Pb 年龄及地球化学数据[J]. 地质通报, 34(Z1): 318-327.
- 康志强, 许继峰, 陈建林, 王保弟, 董彦辉. 2010. 西藏南部桑日群火山岩的时代: 来自晚期马门侵入体的约束[J]. 地球化学, 39(6): 520-530.
- 李华亮, 高成, 李正汉, 张璋, 彭智敏, 关俊雷. 2016. 西藏班公湖地区竟柱山组时代及其构造意义[J]. 大地构造与成矿学, 40(4): 663-673.
- 李晓寒. 2015. 西藏南部仲巴微地体中新世埃达克岩成因及构造意义[D]. 北京: 中国地质大学.
- 莫宣学, 赵志丹, 邓晋福, 董国臣, 周肃, 郭铁鹰, 张双全, 王亮亮. 2003. 印度—亚洲大陆主碰撞过程的火山作用响应[J]. 地学前缘, 10(3): 135-148.
- 莫宣学, 董国臣, 赵志丹, 周肃, 王亮亮, 邱瑞照, 张风琴. 2005. 西藏冈底斯带花岗岩的时空分布特征及地壳生长演化信息[J]. 高校地质学报, 11(3): 281-290.
- 牛晓露, 赵志丹, 莫宣学, DEPAOLO D J, 董国臣, 张双全, 朱弟成, 郭铁鹰. 2006. 西藏日喀则地区德村-昂仁蛇绿岩内基性岩的元素与 Sr-Nd-Pb 同位素地球化学及其揭示的特提斯地幔特征[J]. 岩石学报, 22(12): 2875-2888.
- 潘桂棠, 莫宣学, 侯增谦, 朱弟成, 王立全, 李光明, 赵志丹, 耿全如, 廖忠礼. 2006. 冈底斯造山带的时空结构及演化[J].

- 岩石学报, 22(3): 521-533.
- 潘桂棠, 王立全, 朱弟成. 2004. 青藏高原区域地质调查中几个重大科学问题的思考[J]. 地质通报, 23(1): 12-19.
- 宋志伟, 郑常青, 林波, 徐学纯, 梁琛岳, 陈龙, 赵英利, 温泉波. 2021. 辽西寺儿堡-白塔盆地晚侏罗世火山岩地质特征及其对燕山运动的响应[J]. 地球科学, <https://kns.cnki.net/kcms/detail/42.1874.P.20211126.1436.005.html>.
- 吴昌坦. 2019. 西藏冈底斯带埃达克岩岩石成因与斑岩铜成矿潜力研究[D]. 北京: 中国地质大学.
- 王金丽, 张泽明, 董昕, 刘峰, 于飞, 王伟, 徐方建, 沈昆. 2009. 西藏拉萨地体南部晚白垩纪石榴石二辉麻粒岩的发现及其构造意义[J]. 岩石学报, 25(7): 1695-1706.
- 王强, 许继峰, 赵振华, 资锋, 唐功建, 贾小辉, 姜子琦. 2008. 埃达克质岩的构造背景与岩石组合[J]. 矿物岩石地球化学通报, 27(4): 344-350.
- 王旭辉, 郎兴海, 邓煜霖, 谢富伟, 娄渝明, 张赫, 杨宗耀. 2019. 西藏拉萨地体南缘汤白地区始新世辉绿岩脉——新特提斯洋壳断离的证据[J]. 中国地质, 46(6): 1336-1355.
- 王珍珍, 刘栋, 赵志丹, 闫晶晶, 石卿尚, 莫宣学. 2017. 冈底斯带南部桑日高分异I型花岗岩的岩石成因及其动力学意义[J]. 岩石学报, 33(8): 2479-2493.
- 吴旌, 徐亚东, 安显银, 孔令耀, 罗亮, 张克信. 2014. 冈底斯新元古代-中生代沉积盆地演化[J]. 地球科学(中国地质大学学报), 39(8): 1052-1064.
- 西藏自治区地质调查院. 2018a. 1: 50000 区域地质调查报告乃东县幅(H45C003002)[R]. 拉萨: 西藏自治区地质调查院.
- 西藏自治区地质调查院. 2018b. 1: 50000 区域地质调查报告桑日县幅(H45C003004)[R]. 拉萨: 西藏自治区地质调查院.
- 西藏自治区地质调查院. 2003. 1:250000 区域地质调查报告日喀则市幅(H45C003004)[R]. 拉萨: 西藏自治区地质调查院.
- 许志琴, 杨经绥, 李海兵, 鲍少丞, 张泽明, 刘焰. 2011. 印度-亚洲碰撞大地构造[J]. 地质学报, 85(1): 1-33.
- 闫国强, 丁俊, 黄勇, 王欣欣, 张凯. 2014. 西藏山南比马组安山岩形成时代及意义[J]. 金属矿山, 458(8): 91-94.
- 杨宗耀, 胡古月, 肖洪天, 王鹰, 赵晓彦. 2019. 西藏汤白矿区下白垩统比马组砂岩地球化学特征: 对冈底斯南缘构造演化的启示[J]. 岩石学报, 35(7): 2189-2205.
- 叶丽娟, 赵志丹, 刘栋, 朱弟成, 董国臣, 莫宣学, 胡兆初, 刘勇胜. 2015. 西藏南木林晚白垩世辉绿岩与花岗质脉岩成因及其揭示的伸展背景[J]. 岩石学报, 31(5): 1298-1312.
- 张旗, 王焰, 钱青, 杨进辉, 王元龙, 赵太平, 郭光军. 2001. 中国东部燕山期埃达克岩的特征及其构造-成矿意义[J]. 岩石学报, 17(2): 236-244.
- 张玉涛, 张连昌, 英基丰, 周新华, 王非, 侯泉林, 刘庆. 2007. 大兴安岭北段塔河地区早白垩世火山岩地球化学及源区特征[J]. 岩石学报, 23(11): 2811-2822.
- 张泽明, 丁慧霞, 董昕, 田作林. 2019. 冈底斯岩浆弧的形成与演化[J]. 岩石学报, 35(2): 275-294.

## References:

- BAO Zhi-wei, ZHAO Zhen-hua, GUHA J, WILLIAMS-JONES A E. 2004. HFSE, REE, and PGE geochemistry of three sedimentary rock-hosted disseminated gold deposits in southwestern Guizhou Province, China[J]. Geochemical Journal, 38: 363-381.
- CHEN Lei, QIN Ke-zhang, LI Guang-ming, LI Jin-xiang, XIAO Bo, ZHAO Jun-xing, FAN Xin. 2015. Zircon U-Pb ages, geochemistry, and Sr-Nd-Pb-Hf isotopes of the Nuri intrusive rocks in the Gangdese area, southern Tibet: Constraints on timing, petrogenesis, and tectonic transformation[J]. Lithos, 212-215: 379-396.
- CHEN Xi-lian, RICHARDS J P, LIANG Hua-ying, ZOU Yin-qiao, ZHANG Jian, HUANG Wen-ting, REN Long, WANG Fang-yue. 2019. Contrasting arc magma fertilities in the Gangdese belt, Southern Tibet: Evidence from geochemical variations of Jurassic volcanic rocks[J]. Lithos, 324-325: 789-802.
- CHUNG Sun-lin, CHU Mei-fei, ZHANG Yu-quan, XIE Ying-wen, LO Ching-hua, LEE Tung-yi, LAN Ching-ying, LI Xian-hua, ZHANG Qi, WANG Yi-zhao. 2005. Tibetan tectonic evolution inferred from spatial and temporal variations in post-collisional magmatism[J]. Earth Science Reviews, 68(3-4): 173-196.
- CHUNG Sun-lin, LIU Dun-yi, JI Jian-qing, CHU Mei-fei, LEE Hao-yang, WEN Da-jen, LO Ching-hua, LEE Tung-yi, QIAN Qing, ZHANG Qi. 2003. Adakites from continental collision zones: Melting of thickened lower crust beneath southern Tibet[J]. Geology, 31(11): 1021-1024.
- CHUNG Sun-lin, CHU Mei-fei, JI Jian-qing, O'REILLY S Y, PEARSON N J, LIU Dun-yi, LEE Tung-yi, LO Ching-hua. 2009. The nature and timing of crustal thickening in Southern Tibet: Geochemical and zircon Hf isotopic constraints from postcollisional adakites[J]. Tectonophysics, 477(1-2): 36-48.
- CORFU F, HANCHAR J M, HOSKIN P W O, KINNY P. 2003. Atlas of zircon textures[J]. Reviews in Mineralogy and Geochemistry, 53: 469-500.
- DAI Zuo-wen, LI Guang-ming, DING Jun, HUANG Yong, CAO Hua-wen. 2018. Late Cretaceous adakite in Nuri area, Tibet: Products of ridge subduction[J]. Earth Science, 43(8): 2727-2741(in Chinese with English abstract).
- DEFANT M J, DRUMMOND M S. 1990. Derivation of some modern arc magmas by melting of young subducted lithosphere[J]. Nature, 347(6294): 662-665.
- DRUMMOND M S, DEFANT M J, KEPEZHINSKAS P K. 1996. The petrogenesis of slab-derived trondhjemite-tonalite-dacite/adakite magmas[J]. Special Paper of the Geological Society of America, 315: 205-215.
- ENGLAND P, HOUSEMAN G. 1986. Finite strain calculations of continental deformation: 2. Comparison with the India-Asia Collision Zone[J]. Journal of Geophysical Research Solid Earth, 91(B3): 3664-3676.
- FANG Xiang, TANG Ju-xing, SONG Yang, YANG Chao, DING Shuai, WANG Yi-yun, WANG Qin, SUN Xing-guo, LI Yu-bin, WEI Lu-jie, ZHANG Zhi, YANG Huan-huan, GAO Ke, TANG Pan. 2015. Formation epoch of the South Tiegelong supelarge epithermal Cu (Au-Ag) deposit in Tibet and its geological implications[J]. Acta Geoscientica Sinica, 36(2): 168-172(in Chinese with English abstract).
- FROST B R, BARNES C G, GOLLINS W J, ARCUS R J, ELLIS D J, FROST C D. 2001. A geochemical classification for granitic rocks[J]. Journal of Petrology, 42(11): 2033-2048.
- GENG Hong-yan, SUN Min, YUAN Chao, XIAO Wen-jiao, XIAN Wei-sheng, ZHAO Guo-chun, ZHANG Li-fei, WONG K, WU Fu-yuan. 2009. Geochemical, Sr-Nd and zircon U-Pb-Hf isotopic studies of Late Carboniferous magmatism in the West Junggar, Xinjiang: Implications for ridge subduction?[J].

- Chemical Geology, 266(3-4): 364-389.
- GAO Teng, WANG Li-qiang, WANG Yong, ZHENG Si-lun, HU Yu. 2019. Zircon U-Pb age, Hf isotope and geochemistry of quartz diorite porphyry of the Jiangmanan copper-silver ore district in the western part of the Bangong Co-Nujiang metallogenic belt[J]. *Acta Geoscientica Sinica*, 40(6): 884-894(in Chinese with English abstract).
- GORTON M P, SCHANDL E S. 2000. From continents to island arcs: A geochemical index of tectonic setting for arc-related and within-plate felsic to intermediate volcanic rocks[J]. *Canada Mineral*, 38: 1065-1073.
- GUAN Qi, ZHU Di-cheng, ZHAO Zhi-dan, ZHANG Liang-liang, LIU Min, LI Xiao-wei, YU Feng, MO Xuan-xue. 2010. Late Cretaceous adakites in the eastern segment of the Gangdese Belt, southern Tibet: Products of Neo-Tethyan ridge subduction?[J]. *Acta Petrologica Sinica*, 26(7): 2165-2179(in Chinese with English abstract).
- GUAN Qi, ZHU Di-cheng, ZHAO Zhi-dan, DONG Guo-chen, MO Xuan-xue, LIU Yong-sheng, HU Zhao-chu, YUAN Hong-lin. 2011. Zircon U-Pb chronology, geochemistry of the Late Cretaceous mafic magmatism in the southern Lhasa Terrane and its implications[J]. *Acta Petrologica Sinica*, 27(7): 2083-2094(in Chinese with English abstract).
- HAO Lu-lu, WANG Qiang, WYMAN D A, QU Quan, DAN Wei, JIANG Zi-qi, WU Fu-yuan, YANG Jin-hui, LONG Xiao-ping, LI Jie. 2015. Underplating of basaltic magmas and crustal growth in a continental arc: Evidence from Late Mesozoic intermediate-felsic intrusive rocks in southern Qiangtang, central Tibet[J]. *Lithos*, 245: 223-242.
- HARRIS N B W, PEARCE J A, TINDLE A G. 1986. Geochemical characteristics of collision zone magmatism[J]. Geological Society, London, Special Publication, 19: 67-81.
- HASTIE A R, KERR A C, PEARCE J A, MITCHELL S F. 2007. Classification of altered volcanic island arc rocks using immobile trace elements: Development of the Th-Co discrimination diagram[J]. *Journal of Petrology*, 48(12): 2341-2357.
- HE Qing, LANG Xing-hai, LI Liang, CHEN Cui-hua, WANG Xu-hui, DENG Yu-lin, YIN Qing, XIE Fu-Wei, YANG Zong-yao, ZHANG Zhong, JIANG Kai. 2020. U-Pb zircon age and geochemistry of the Cuocun gabbro in the southern Lhasa Terrane: Implications for Early Cretaceous rollback of the Neo-Tethyan oceanic slab[J]. *Geological Journal*, 56(3): 1424-1444.
- HOU Zeng-qian, MO Xuan-xue, GAO Yong-fei, YANG Zhi-ming, DONG Guo-chen, DING Lin. 2006. Early processes and tectonic model for the Indian—Asian Continental Collision: Evidence from the Cenozoic Gangdese igneous rocks in Tibet[J]. *Acta Geologica Sinica*, 80(9): 1233-1248(in Chinese with English abstract).
- HUANG Feng, XU Ji-feng, CHEN Jian-lin, KANG Zhi-jiang, DONG Yan-hui. 2015. Early Jurassic volcanic rocks from the Yeba Formation and Sangri Group: Products of continental marginal arc and intra-oceanic arc during the subduction of Neo-Tethys Ocean?[J]. *Acta Petrologica Sinica*, 31(7): 2089-2100(in Chinese with English abstract).
- HUANG Tong-tong, XU Ji-feng, CHEN Jian-lin, WU Jian-bin, ZENG Yun-chuan. 2016. Sedimentary record of Jurassic northward subduction of the Bangong-Nujiang Ocean: insights from detrital zircons[J]. *International Geology Review*, 59(2): 166-184.
- HUANG Yu, ZHAO Zhi-dan, ZHANG Feng-qin, ZHU Di-cheng, DONG Guo-chen, ZHOU Shu-ran, MO Xuan-xue. 2010. Geochemistry and implication of the Gangdese batholiths from Renbu and Lhasa areas in southern Gangdese, Tibet[J]. *Acta Petrologica Sinica*, 26(10): 3131-3142(in Chinese with English abstract).
- JI Wei-qiang, WU Fu-yuan, CHUNG Sun-lin, LI Jin-xiang, LIU Chuan-zhou. 2009. Zircon U-Pb geochronology and HF isotopic constraints on petrogenesis of the Gangdese batholith, southern Tibet[J]. *Chemical Geology*, 262(3-4): 229-245.
- JIANG Zi-qi, WANG Qiang, LI Zheng-xiang, WYMAN D A, TANG Gong-jian, JIA Xiao-hui, YANG Yue-heng. 2012. Late Cretaceous (ca. 90 Ma) adakitic intrusive rocks in the Kelu area, Gangdese Belt (southern Tibet): Slab melting and implications for Cu-Au mineralization[J]. *Journal of Asian Earth Sciences*, 53(2): 67-81.
- JIANG Zi-qi, WANG Qiang, WYMAN D A, LI Zheng-xiang, YANG Jin-hui, SHI Xiao-bing, MA Lin, TANG Gong-jian, GOU Guo-ning, JIA Xiao-hui, GUO Hai-feng. 2014. Transition from oceanic to continental lithosphere subduction in southern Tibet: Evidence from the Late Cretaceous-Early Oligocene (ca. 91-30 Ma) intrusive rocks in the Chanang-Zedong area, southern Gangdese[J]. *Lithos*, 196-197: 213-231.
- KANG Zhi-jiang, XU Ji-feng, WILDE S A, FENG Zuo-hai, CHEN Jian-lin, WANG Bao-di, FU Wen-chun, PAN Hui-bin. 2014. Geochronology and geochemistry of the Sangri Group Volcanic Rocks, Southern Lhasa Terrane: Implications for the early subduction history of the Neo-Tethys and Gangdese Magmatic Arc[J]. *Lithos*, 200-201: 157-168.
- KANG Zhi-jiang, XU Ji-feng, CHEN Jian-lin, WANG Bao-di, DONG Yan-hui. 2010. The geochronology of Sangri Group volcanic rocks in Tibet: Constraints from later Mamen intrusions[J]. *Geochimica*, 39(6): 520-530(in Chinese with English abstract).
- KANG Zhi-jiang, FU Wen-chun, TIAN Guang-hao. 2015. A discussion on Mesozoic volcanic stratigraphic sequence in Sangri County, Tibet: evidence from zircon U-Pb ages and geochemical compositions[J]. *Geological Bulletin of China*, 34(Z1): 318-327(in Chinese with English abstract).
- KAPP P, MURPHY M A, YIN A, HARRISON T M, DING L, GUO J H. 2003. Mesozoic and Cenozoic tectonic evolution of the Shiquanhe area of western Tibet[J]. *Tectonics*, 22(4): 3-1-3-24.
- KAY R W, KAY S M. 1993. Delamination and delamination magmatism[J]. *Tectonophysics*, 219(1-3): 177-189.
- LANG Xing-hai, DENG Yu-lin, WANG Xu-hui, TANG Ju-xing, YIN Qing, XIE Fu-wei, YANG Zong-yao, LI Zhuang, HE Qing, LI Liang, ZHANG Zhong, JIANG Kai. 2020. Geochronology and geochemistry of volcanic rocks of the Bima Formation, southern Lhasa subterrane, Tibet: Implications for early Neo-Tethyan subduction[J]. *Gondwana Research*, 80: 335-349.
- LANG Xing-hai, LIU Dong, DENG Yu-lin, TANG Ju-xing, XIE Fu-wei, YANG Zong-yao, CUI Zhi-wei, WANG Xu-hui, LI Zhi-jun, ZHANG Zhong, ZHANG Jin-shu, HUANG Yong.

2018. New discovery of the 341 Ma gabbro at Xiongcun district in the southern margin of Lhasa Terrane, Tibet[J]. *Acta Geologica Sinica (English Edition)*, 92(1): 420-421.
- LANG Xing-hai, WANG Xu-hui, DENG Yu-lin, TANG Ju-xing, XIE Fu-wei, ZHOU You, HUANG Yong, LI Zhuang, YIN Qing, JIANG Kai. 2019. Early Jurassic volcanic rocks in the Xiongcun district, southern Lhasa subterrane, Tibet: Implications for the tectono-magmatic events associated with the early evolution of the Neo-Tethys Ocean[J]. *Lithos*, 340-341: 166-180.
- LI Xiao-han. 2015. Miocene adakitic intrusive in the Zhongba microterrane of southern Tibet: Implications for origin and tectonics[D]. Beijing: China University of Geosciences(in Chinese with English abstract).
- LI Hua-liang, GAO Cheng, LI Zheng-han, ZHANG Zhang, PENG Zhi-min, GUAN Jun-lei. 2016. Age and tectonic significance of Jingzhushan Formation in Bangong Lake area, Tibet[J]. *Geotectonica et Metallogenesis*, 40(4): 663-673(in Chinese with English abstract).
- LI Liang, XIE Hui, LANG Xing-hai, WANG Xu-hui, HE Qing, DENG Yu-lin, XIE Fu-wei. 2021. Petrogenesis of Early-Middle Jurassic garbbros in southern Tibet with implications for crustal growth in the southern Lhasa subterrane[J]. *International Geology Review*, DOI: 10.1080/00206814.2021.1961102.
- LIU Yong-sheng, HU Zhao-chu, ZONG Ke-qing, GAO Chang-gui, GAO Shan, XU Juan, CHEN Hai-hong. 2010. Reappraisal and refinement of zircon U-Pb isotope and trace element analyses by LA-ICP-MS[J]. *Chinese Science Bulletin*, 55(15): 1535-1546.
- MA Xu-xuan, XU Zhi-qin, MEERT J G, SANTOSH M. 2017. Early Jurassic intra-oceanic arc system of the Neotethys Ocean: Constraints from andesites in the Gangdese magmatic belt, south Tibet[J]. *Island Arc*, 26(5): e12202.
- MACPHERSON C G, DREHER S T, THIRLWALL M F. 2006. Adakites without slab melting: High pressure differentiation of island arc magma, Mindanao, the Philippines[J]. *Earth and Planetary Science Letters*, 243(3-4): 581-593.
- MA Lin, WANG Qiang, LI Zheng-xiang, WYMAN D A, JIANG Zi-qi, YANG Jin-hui, GOU Guo-ning, GUO Hai-feng. 2013a. Early Late Cretaceous(ca.93 Ma) norites and hornblendites in the Milin area, eastern Gangdese: Lithosphere-asthenosphere interaction during slab roll-back and an insight into early Late Cretaceous(ca.100-80Ma) magmatic “flare-up” in southern Lhasa(Tibet)[J]. *Lithos*, 172-173: 17-30.
- MA Lin, WANG Qiang, WYMAN D A, LI Zheng-xiang, JIANG Zi-qi, YANG Jin-hui, GOU Guo-ning, GUO Hai-feng. 2013b. Late Cretaceous(100-89 Ma) magnesian charnockites with adakitic affinities in the Milin area, eastern Gangdese: Partial melting of subduction oceanic crust and implications for crustal growth in southern Tibet[J]. *Lithos*, 175-176: 315-332.
- MARTIN H, SMITHIES R H, RAPP R, MOYEN J F, CHAMPION D. 2005. An overview of adakite, tonalite trondhjemite-granodiorite (TTG), and sanukitoid: relationships and some implications for crustal evolution[J]. *Lithos*, 79(1-2): 1-24.
- MO Xuan-xue, DONG Guo-chen, ZHAO Zhi-dan, GUO Tie-ying, WANG Liang-liang, CHEN Tao. 2005. Timing of magma mixing in the Gangdese magmatic belt during the India-Asia collision: Zircon SHRIMP U-Pb dating[J]. *Acta Geologica Sinica (English Edition)*, 79(1): 66-76.
- MO Xuan-xue, DONG Guo-chen, ZHAO Zhi-dan, ZHOU Su, WANG Liang-liang, QIU Rui-zhao, ZHANG Feng-qin. 2005. Spatial and temporal distribution and characteristics of Granitoids in the Gangdese, Tibet and implication for crustal growth and evolution[J]. *Geological Journal of China Universities*, 11(3): 281-290(in Chinese with English abstract).
- MO Xuan-xue, HOU Zeng-qian, NIU Yao-ling, DONG Guo-chen, QU Xiao-ming, ZHAO Zhi-dan, YANG Zhi-ming. 2007. Mantle contributions to crustal thickening during continental collision: Evidence from Cenozoic igneous rocks in southern Tibet[J]. *Lithos*, 96(1-2): 225-242.
- MO Xuan-xue, ZHAO Zhi-dan, DENG Jin-fu, DONG Guo-chen, ZHOU Su, GUO Tie-ying, ZHANG Shuang-quan, WANG Liang-liang. 2003. Response of volcanism to the India-Asia collision[J]. *Earth Science Frontiers*, 10(3): 135-148(in Chinese with English abstract).
- NIU Xiao-lu, ZHAO Zhi-dan, MO Xuan-xue, DEPAOLO D J, DONG Guo-chen, ZHANG Shuang-quan, ZHU Di-cheng, GUO Tie-ying. 2006. Elemental and Sr-Nd-Pb isotopic geochemistry for basic rocks from Decun-Angren ophiolites in Xigaze area, Tibet: implications for the characteristics of the Tethyan upper mantle domain[J]. *Acta Petrologica Sinica*, 22(12): 2875-2888(in Chinese with English abstract).
- OTHMAN D B, WHITE W M, PATCHETT J. 1989. The geochemistry of marine sediments, island arc magma genesis, and crust-mantle recycling[J]. *Earth and Planetary Science Letters*, 94(1-2): 1-21.
- PAN Gui-tang, MO Xuan-xue, HOU Zeng-qian, ZHU Di-cheng, WANG Li-quan, LI Guang-ming, ZHAO Zhi-dan, GENG Quan-ru, LIAO Zhong-li. 2006. Spatial-temporal framework of Gangdese Orogenic Belt and its evolution[J]. *Acta Petrologica Sinica*, 22(3): 521-533(in Chinese with English abstract).
- PAN Gui-tang, WANG Li-quan, ZHU Di-cheng. 2004. Thoughts on some important scientific problems in regional geological survey of the Qinghai-Tibet Plateau[J]. *Geological Bulletin of China*, 23(1): 12-19(in Chinese with English abstract).
- PEARCE J, HARRIS N, TINDLE A. 1984. Trace element discrimination diagrams for the tectonic interpretation of granitic rocks[J]. *Journal of Petrology*, 25(4): 956-983.
- PROUTEAU G, SCAILLET B, PICHAVENT M, MAURY R. 2001. Evidence for mantle metasomatism by hydrous silicic melts derived from subducted oceanic crust[J]. *Nature*, 410(6825): 197-200.
- QIN Jiang-feng, LAI Shao-cong, WANG Juan, LI Yong-feng. 2007. High-Mg<sup>#</sup> adakitic tonalite from the Xichahe area, South Qinling Orogenic Belt (Central China): petrogenesis and geological implications[J]. *International Geology Review*, 49(12): 1145-1158.
- RAPP R P, WATSON E B. 1995. Dehydration melting of metabasalt at 8-32 kbar: Implications for continental growth and crust-mantle recycling[J]. *Journal of Petrology*, 36(4): 891-931.
- RAPP R P, SHIMIZU N, NORMAN M D, APPLEGATE G S. 1999. Reaction between slab-derived melts and peridotite in the mantle wedge: experimental constraints at 3.8 GPa[J]. *Chemical Geology*, 160(4): 335-356.

- RAN Meng-lan, KANG Zhi-qiang, XU Ji-feng, YANG Feng, JIANG Zi-qi, LI Qiang, WEI Nai-shao, WEI Tian-wei, LIU Di. 2019. Evolution of the northward subduction of the Neo-Tethys: Implications of geochemistry of Cretaceous arc volcanics in Qinghai-Tibetan Plateau[J]. *Palaeogeography, Palaeoclimatology, Palaeoecology*, 515: 83-94.
- RICKWOOD P C. 1989. Boundary lines within petrologic diagrams which use oxides of major and minor elements[J]. *Lithos*, 22(4): 247-263.
- SEN C, DUNN T. 1994. Dehydration melting of a basaltic composition amphibolite at 1.5 and 2.0 GPa: implication for the origin of adakites[J]. *Contributions to Mineralogy and Petrology*, 117(4): 394-409.
- SMITHIES R H. 2000. The Archaean tonalite—trondhjemite—granodiorite (TTG) series is not an analogue of Cenozoic adakite[J]. *Earth and Planetary Science Letters*, 182(1): 115-125.
- SONG Zhi-wei, ZHENG Chang-qing, LIN Bo, XU Xue-chun, LIANG Chen-yue, CHEN Long, ZHAO Ying-li, WEN Quan-bo. 2021. Geological characteristics of Late Jurassic volcanic rocks in Sierbao-Baita Basin, Western Liaoning Province and its response to Yanshan Movement[J]. *Earth Science*, <https://kns.cnki.net/kcms/detail/42.1874.P.20211126.1436.005.html>(in Chinese with English abstract).
- STERN C R, KILIAN R. 1996. Role of the subducted slab, mantle wedge and continental crust in the generation of adakites from the Andean Austral Volcanic Zone[J]. *Contributions to Mineralogy and Petrology*, 123(3): 263-281.
- STRECK M J, LEEMAN W P, CHESLEY J. 2007. High-magnesian andesite from Mount Shasta: A product of magma mixing and contamination, not a primitive mantle melt[J]. *Geology*, 35(4): 351-354.
- SUN S S, McDONOUGH W S. 1989. Chemical and isotopic systematics of oceanic basalts: Implications for mantle composition and processes[J]. Geological Society, London, Special Publication, 42(1): 313-345.
- TANG Ming, JI Wei-qiang, CHU Xu, WU An-bin, CHEN Chen. 2020. Reconstructing crustal thickness evolution from europium anomalies in detrital zircons[J]. *Geology*, 49(1): 76-80.
- The Geological Survey of Tibet Autonomous Region. 2018. The Report of Regional geological survey of Naidong Sheet at the scale of 1:50000[R]. Lhasa: The Geological Survey of Tibet Autonomous Region(in Chinese).
- The Geological Survey of Tibet Autonomous Region. 2018. The Report of Regional geological survey of Sangri Sheet at the scale of 1:50000[R]. Lhasa: The Geological Survey of Tibet Autonomous Region(in Chinese).
- The Geological Survey of Tibet Autonomous Region. 2003. The Report of Regional geological survey of Rikaze Sheet at the scale of 1:50000[R]. Lhasa: The Geological Survey of Tibet Autonomous Region(in Chinese).
- WANG Jin-li, ZHANG Ze-ming, DONG Xin, LIU Feng, YU Fei, WANG Wei, XU Fang-jian, SHEN Kun. 2009. Discovery of Late Cretaceous garnet two-pyroxene granulite in the southern Lhasa terrane, Tibet and its tectonic significances[J]. *Acta Petrologica Sinica*, 25(7): 1695-1706(in Chinese with English abstract).
- WANG Qiang, XU Ji-feng, JIAN Ping, BAO Zhi-wei, ZHAO Zhen-huan, LI Chao-feng, XIONG Xiao-lin, MA Jin-long. 2006. Petrogenesis of adakitic porphyries in an extensional tectonic setting, Dexing, South China: Implications for the genesis of porphyry copper mineralization[J]. *Journal of Petrology*, 47(1): 119-144.
- WANG Qiang, XU Ji-feng, ZHAO Zhen-hua, ZI Feng, TANG Gong-jian, JIA Xiao-hui, JIANG Zi-qi. 2008. Tectonic setting and associated rock suites of adakitic rocks[J]. *Bulletin of Mineralogy, Petrology and Geochemistry*, 27(4): 344-350(in Chinese with English abstract).
- WANG Xu-hui, LANG Xing-hai, DENG Yu-lin, XIE Fu-wei, LOU Yu-ming, ZHANG He, YANG Zong-yao. 2019. Eocene diabase dikes in the Tangbai area, southern margin of Lhasa terrane, Tibet: Evidence for the slab break-off of the Neo-Tethys Ocean[J]. *Geology in China*, 46(6): 1336-1355(in Chinese with English abstract).
- WANG Xu-hui, LANG Xing-hai, TANG Ju-xing, DENG Yu-lin, HE Qing, XIE Fu-wei, LI Liang, YIN Qing, LI Zhi-jun, LI Zhuang, YANG Zong-yao, DONG Shu-yi, DING Feng, WANG Zi-zheng, HUANG Yong. 2020. Early Carboniferous back-arc rifting-related magmatism in southern Tibet: Implications for the history of the Lhasa terrane separation from Gondwana[J]. *Tectonics*, 39(10): e2020TC006237.
- WANG Xu-hui, LANG Xing-hai, TANG Ju-xing, DENG Yu-lin, CUI Zhi-wei. 2019. Early–Middle Jurassic (182–170 Ma) Ruocuo adakitic porphyries, southern margin of the Lhasa terrane, Tibet: Implications for geodynamic setting and porphyry Cu–Au mineralization[J]. *Journal of Asian Earth Sciences*, 173: 336-351.
- WANG Zhen-zhen, LIU Dong, ZHAO Zhi-dan, YAN Jing-jing, SHI Qing-shang, MO Xuan-xue. 2017. The Sangri highly fractionated I-type granites in southern Gangdese: Petrogenesis and dynamic implication[J]. *Acta Petrologica Sinica*, 33(8): 2479-2493(in Chinese with English abstract).
- WEIS D, KIEFFEER B, MAERSCHALK C, BARLING J, JONG J D, WILLIAMS G A, HANANO D, PRETORIUS W, MATTIELLI N, SCOATES J S, GOOLAERTS A, FRIEDMAN R M, MAHONEY J B. 2006. High-precision isotopic characterization of USGS reference materials by TIMS and MC-ICP-MS[J]. *Geochemistry Geophysics Geosystems*, 7(8): 1-30.
- WEN Da-ren, CHUNG Sun-lin, SONG Biao, LIZUKA Y, YANG Huan-jen, JI Jian-qing, LIU D Y, GALLET S. 2008a. Late Cretaceous Gangdese intrusions of adakitic geochemical characteristics, SE Tibet: Petrogenesis and tectonic implications[J]. *Lithos*, 105(1-2): 1-11.
- WEN Da-ren, LIU Dun-yi, CHUNG Sun-lin, CHU Mei-fei, JI Jian-qing, ZHANG Qi, SONG Biao, LEE T Y, YEH M W, LO Ching-hua. 2008b. Zircon SHRIMP U-Pb ages of the Gangdese Batholith and implications for Neotethyan subduction in southern Tibet[J]. *Chemical Geology*, 252(3-4): 191-201.
- WINCHESTER J A, FLOYD P A. 1977. Geochemical discrimination of different magma series and their differentiation products using immobile elements[J]. *Chemical Geology*, 20: 325-343.
- WOOD D A. 1979. The application of a Th—Hf—Ta diagram to problems of tectonomagmatic classification and to establishing the nature of crustal contamination of basaltic lavas of the

- British Tertiary Volcanic Province[J]. *Earth and Planetary Science Letters*, 50(1): 11-30.
- WU Chang-da. 2019. Petrogenesis of adakites and its potential for porphyry copper mineralization in Gangdese belt, Tibet[D]. Beijing: China University of Geosciences(Beijing)(in Chinese).
- WU Jing, XU Ya-dong, AN Xian-yin, KONG Ling-yao, LUO Li-ang, ZHANG Ke-xin. 2014. Evolution of Neoproterozoic-Mesozoic sedimentary basins in Gangdese area, Tibetan Plateau[J]. *Earth Science(Journal of China University of Geoscience)*, 39(8): 1052-1064(in Chinese with English abstract).
- WU Yuan-bao, ZHENG Yong-fei. 2004. Genesis of zircon and its constraints on interpretation of U-Pb age[J]. *Chinese Science Bulletin*, 49: 1554-1569.
- XU Ji-feng, CASTILLO P R. 2004. Geochemical and Nd-Pb isotopic characteristics of the Tethyan asthenosphere: Implications for the origin of the Indian Ocean mantle domain[J]. *Tectonophysics*, 393(1-4): 9-27.
- XU Zhi-qin, YANG Jing-sui, LI Hai-bing, JI Shao-cheng, ZHANG Ze-ming, LIU Yan. 2011. On the tectonics of the India-Asia Collision[J]. *Acta Geologica Sinica*, 85(1): 1-33(in Chinese with English abstract).
- YAN Guo-qiang, DING Jun, HUANG Yong, WANG Xin-xin, ZHANG Kai. 2014. Geochronology and significances of Bima Formation andesite of Shannan, Tibet[J]. *Metal Mine*, 458(8): 91-94(in Chinese with English abstract).
- YANG Zong-yao, HU Gu-yue, XIAO Hong-tian, WANG Ying, ZHAO Xiao-yan. 2019. Geochemical characteristics of the Early Cretaceous sandstones from the Tangbai deposit, Tibet: Implications for the tectonic evolution of the southern margin of the Gangdese[J]. *Acta Petrologica Sinica*, 35(7): 2189-2205(in Chinese with English abstract).
- YANG Zong-yao, TANG Ju-xing, SANTOSH M, ZHAO Xiao-yan, LANG Xing-hai, WANG Ying, DING Shuai, RAN Feng-qin. 2021. Microcontinent subduction and S-type volcanism prior to India-Asia collision[J]. *Scientific Reports*, 11: 14882.
- YE Li-juan, ZHAO Zhi-dan, LIU Dong, ZHU Di-cheng, DONG Guo-chen, MO Xuan-xue, HU Zhao-chu, LIU Yong-sheng. 2015. Late Cretaceous diabase and granite dike in Namling, Tibet: Petrogenesis and implications for extension[J]. *Acta Petrologica Sinica*, 31(5): 1298-1312(in Chinese with English abstract).
- YIN A, HARRISON T M. 2000. Geologic evolution of the Himalayan-Tibetan orogen[J]. *Annual Review of Earth and Planetary Sciences*, 28: 211-280.
- ZHANG Qi, WANG Yan, QIAN Qing, YANG Jin-hui, WANG Yuan-long, ZHAO Tai-ping, GUO Guang-jun. 2001. The characteristics and tectonic-metallogenetic significances of the adakites in Yanshan period from eastern China[J]. *Acta Petrologica Sinica*, 17(2): 236-244(in Chinese with English abstract).
- ZHANG Yu-tao, ZHANG Lian-chang, ZHOU Xin-hua, WANG Fei, HOU Quan-lin, LIU Qing. 2007. Geochemistry and source characteristics of early Cretaceous volcanic rocks in Tahe, north Da Hinggan Mountain[J]. *Acta Petrologica Sinica*, 23(11): 2811-2822(in Chinese with English abstract).
- ZHANG Ze-ming, DING Hui-xia, DONG Xin, TIAN Zuo-lin. 2019. Formation and evolution of the Gangdese magmatic arc, southern Tibet[J]. *Acta Petrologica Sinica*, 35(2): 275-294(in Chinese with English abstract).
- ZHANG Ze-ming, ZHAO Guo-chun, SANTOSH M, WANG Jin-li, DONG Xin, SHEN Kun. 2010. Late Cretaceous charnockite with adakitic affinities from the Gangdese batholith, southeastern Tibet: Evidence for Neo-Tethyan mid-ocean ridge subduction[J]. *Gondwana Research*, 17(4): 615-631.
- ZHANG Liang-liang, ZHU Di-cheng, WANG Qing, ZHAO Zhi-dan, LIU Dong, XIE Jin-cheng. 2018. Late Cretaceous volcanic rocks in the Sangri area, southern Lhasa Terrane, Tibet: Evidence for oceanic ridge subduction[J]. *Lithos*, 326-327: 144-157.
- ZHANG Shuang-quan, MAHONEY J J, MO Xuan-xue, GHAZI A M, MILANI L, CRAWFORD A J, GUO T Y, ZHAO Zhi-dan. 2005. Evidence for a widespread Tethyan upper mantle with Indian-Ocean-type isotopic characteristics[J]. *Journal of Petrology*, 46(4): 829-858.
- ZHENG Yuan-chuan, HOU Zeng-qian, GONG Ying-li, LIANG Wei, SUN Qin-zhong, ZHANG Song, FU Qiang, HUANG Ke-xian, LI Qiu-yun, LI Wei. 2014. Petrogenesis of Cretaceous adakite-like intrusions of the Gangdese Plutonic Belt, southern Tibet: Implications for mid-ocean ridge subduction and crustal growth[J]. *Lithos*, 190-191: 240-263.
- ZHU Di-cheng, ZHAO Zhi-dan, PAN Gui-tang, LEE Hao-yang, KANG Zhi-jiang, LIAO Zhong-li, WANG Li-quan, LI Guang-ming, DONG Guo-chen, LIU Bo. 2009. Early cretaceous subduction-related adakite-like rocks of the Gangdese Belt, southern Tibet: Products of slab melting and subsequent melt-peridotite interaction[J]. *Journal of Asian Earth Sciences*, 34(3): 298-309.
- ZHU Di-cheng, ZHAO Zhi-dan, NIU Yao-ling, MO Xuan-xue, CHUNG Sun-lin, HOU Zeng-qian, WANG Li-quan, WU Fu-yuan. 2011. The Lhasa Terrane: Record of a microcontinent and its histories of drift and growth[J]. *Earth and Planetary Science Letters*, 301(1-2): 241-255.
- ZHU Di-cheng, ZHAO Zhi-dan, NIU Yao-ling, DILEK Y, HOU Zeng-qian, MO Xuan-xue. 2013. The origin and pre-Cenozoic evolution of the Tibetan Plateau[J]. *Gondwana Research*, 23(4): 1429-1454.
- ZHU Di-cheng, WANG Qing, CAWOOD P A, ZHAO Zhi-dan, MO Xuan-xue. 2017. Raising the Gangdese Mountains in southern Tibet[J]. *Journal of Geophysical Research Solid Earth*, 122(1): 214-223.
- ZHU Di-cheng, WANG Qing, CHUNG Sun-lin, CAWOOD P A, ZHAO Zhi-dan. 2018. Gangdese magmatism in southern Tibet and India-Asia convergence since 120 Ma[J]. *Geological Society, London, Special Publication*, 483: 583-604.

附表 1 桑日地区晚白垩世火山岩的锆石 LA-ICP-MS U-Pb 同位素分析结果

Supplementary Table 1 Zircon LA-ICP-MS U-Pb analysis data for Late Cretaceous volcanic rocks in the Sangri area

编号	含量( $\times 10^{-6}$ )				Th/U	同位素比值						年龄/Ma			
	U	Th	$^{206}\text{Pb}^*$			$^{207}\text{Pb}/^{206}\text{Pb}$	$\pm 1\sigma$	$^{207}\text{Pb}/^{235}\text{U}$	$\pm 1\sigma$	$^{206}\text{Pb}/^{238}\text{U}$	$\pm 1\sigma$	$^{206}\text{Pb}/^{238}\text{U}$	$\pm 1\sigma$	$^{207}\text{Pb}/^{235}\text{U}$	$\pm 1\sigma$
Sample (JT07)流纹岩															
1	2042	3753	2896	1.84	0.052 16	0.008 22	0.097 92	0.009 34	0.014 56	0.000 65	93.2	4	94.9	9	98%
2	1507	3041	1667	2.02	0.047 31	0.007 38	0.091 63	0.007 29	0.013 63	0.000 31	87.3	2	89.0	7	98%
3	1199	1805	972	1.51	0.048 21	0.003 91	0.095 10	0.006 12	0.014 11	0.000 38	90.4	2	92.2	6	97%
5	1160	1971	964	1.70	0.048 95	0.003 23	0.094 85	0.003 37	0.014 26	0.000 38	91.3	2	92.0	3	99%
7	1207	1983	1698	1.64	0.050 77	0.009 12	0.099 60	0.004 61	0.014 96	0.000 38	95.7	2	96.4	4	99%
8	812	1008	775	1.24	0.049 07	0.010 44	0.097 92	0.007 95	0.014 67	0.000 32	93.9	2	94.9	7	98%
9	1362	1913	1425	1.40	0.049 53	0.008 46	0.096 20	0.010 63	0.014 37	0.000 45	91.9	3	93.3	10	98%
11	909	1341	714	1.47	0.048 90	0.004 37	0.095 47	0.003 82	0.014 11	0.000 33	90.4	2	92.6	4	97%
12	1363	2458	1734	1.80	0.049 00	0.008 88	0.093 32	0.006 63	0.014 23	0.000 60	91.1	4	90.6	6	99%
13	757	860	610	1.14	0.049 99	0.005 06	0.098 03	0.007 16	0.014 36	0.000 43	91.9	3	95.0	7	96%
14	1457	1810	1025	1.24	0.048 53	0.004 52	0.092 78	0.004 29	0.013 90	0.000 33	89.0	2	90.1	4	98%
15	1066	2186	1274	2.05	0.047 43	0.007 00	0.092 58	0.003 95	0.014 09	0.000 30	90.2	2	89.9	4	99%
16	1658	3161	2037	1.91	0.051 07	0.008 03	0.096 56	0.007 18	0.014 27	0.000 48	91.3	3	93.6	7	97%
17	889	1129	597	1.27	0.048 74	0.005 77	0.096 29	0.003 32	0.014 18	0.000 29	90.8	2	93.3	3	97%
18	1172	1724	1392	1.47	0.051 07	0.006 55	0.094 36	0.009 36	0.014 28	0.000 59	91.4	4	91.6	9	99%
19	1192	1567	799	1.31	0.048 82	0.003 01	0.094 20	0.002 91	0.014 04	0.000 29	89.9	2	91.4	3	98%
20	1697	2370	1254	1.40	0.048 72	0.003 26	0.095 28	0.003 69	0.014 22	0.000 32	91.0	2	92.4	3	98%
21	1149	1818	902	1.58	0.049 58	0.002 85	0.096 00	0.002 50	0.014 02	0.000 31	89.7	2	93.1	2	96%

续附表1

编号	含量( $\times 10^{-6}$ )				同位素比值						年龄/Ma				
	U	Th	$^{206}\text{Pb}^*$	Th/U	$^{207}\text{Pb}/^{206}\text{Pb}$	$\pm 1\sigma$	$^{207}\text{Pb}/^{235}\text{U}$	$\pm 1\sigma$	$^{206}\text{Pb}/^{238}\text{U}$	$\pm 1\sigma$	$^{206}\text{Pb}/^{238}\text{U}$	$\pm 1\sigma$	$^{207}\text{Pb}/^{235}\text{U}$	$\pm 1\sigma$	谐和度
Sample(JT08) 安山岩															
2	1853	3633	1064	1.96	0.048 69	0.001 44	0.095 67	0.003 49	0.014 23	0.000 29	91.1	2	92.8	3	98%
3	974	1508	711	1.55	0.048 95	0.003 67	0.097 36	0.006 84	0.014 24	0.000 39	91.1	3	94.3	6	96%
4	1030	1684	780	1.64	0.049 51	0.002 05	0.098 00	0.004 60	0.014 40	0.000 39	92.2	2	95.0	4	97%
5	689	1316	605	1.91	0.050 55	0.006 16	0.099 88	0.005 06	0.014 38	0.000 39	92.1	2	96.7	5	95%
6	648	2834	603	4.37	0.049 15	0.010 41	0.099 36	0.007 75	0.015 05	0.000 53	96.3	3	96.2	7	99%
7	614	1264	572	2.06	0.049 34	0.003 54	0.097 83	0.005 67	0.014 25	0.000 39	91.2	3	94.8	5	96%
8	456	659	301	1.45	0.048 00	0.002 68	0.096 80	0.006 13	0.014 60	0.000 41	93.4	3	93.8	6	99%
9	695	1315	536	1.89	0.049 33	0.001 68	0.097 32	0.004 01	0.014 31	0.000 36	91.6	2	94.3	4	97%
10	1124	1547	638	1.38	0.049 72	0.001 75	0.099 71	0.004 40	0.014 49	0.000 36	92.7	2	96.5	4	96%
11	416	1296	524	3.11	0.048 71	0.005 61	0.092 56	0.008 89	0.014 12	0.000 47	90.4	3	89.9	8	99%
12	470	662	270	1.41	0.049 88	0.002 34	0.096 98	0.004 28	0.014 15	0.000 33	90.5	2	94.0	4	96%
13	814	1691	713	2.08	0.049 09	0.001 41	0.095 72	0.003 31	0.014 11	0.000 28	90.3	2	92.8	3	97%
14	430	862	383	2.00	0.051 38	0.005 55	0.099 22	0.005 22	0.014 37	0.000 38	92.0	2	96.1	5	95%
15	876	835	613	0.95	0.048 26	0.004 73	0.092 02	0.004 59	0.014 38	0.000 46	92.0	3	89.4	4	97%
16	574	683	422	1.19	0.048 20	0.008 28	0.094 31	0.004 21	0.014 32	0.000 31	91.7	2	91.5	4	99%
17	1061	2530	1264	2.39	0.048 88	0.006 70	0.098 80	0.003 99	0.014 47	0.000 31	92.6	2	95.7	4	96%
18	2413	2826	1286	1.17	0.049 54	0.002 17	0.097 36	0.003 12	0.014 50	0.000 41	92.8	3	94.3	3	98%
20	710	1053	426	1.48	0.048 34	0.001 59	0.094 43	0.003 72	0.014 16	0.000 33	90.6	2	91.6	3	98%

附表 2 桑日地区晚白垩世火山岩主量元素(wt.%)和微量元素( $\times 10^{-6}$ )分析数据表Supplementary Table 2 Analyses of major (wt.%) and trace ( $\times 10^{-6}$ ) elements in Late Cretaceous volcanic rocks in the Sangri area

样品号	JT08-1	JT08-2	JT08-3	JT08-4	JT09-1	JT09-2	JT09-3	JT07-1	JT07-2	JT07-3	JT07-4
								安山岩			
SiO <sub>2</sub>	58.01	64.04	59.22	60.54	57.81	55.79	57.09	73.51	74.26	71.97	70.42
TiO <sub>2</sub>	0.85	0.74	0.89	0.87	0.95	1.07	0.92	0.19	0.21	0.19	0.21
Al <sub>2</sub> O <sub>3</sub>	18.28	16.29	19.19	18.86	16.97	18.83	17.29	13.98	12.75	15.02	16.79
Fe <sub>2</sub> O <sub>3</sub>	6.87	5.52	5.94	6.04	7.46	8.37	7.45	2.55	2.62	2.30	2.68
MnO	0.12	0.09	0.09	0.09	0.11	0.09	0.11	0.05	0.06	0.05	0.05
MgO	3.28	3.12	3.07	3.42	3.68	4.34	3.61	1.65	1.57	1.31	1.57
CaO	7.90	5.21	5.48	4.64	5.35	3.21	5.62	1.36	2.12	2.02	1.76
Na <sub>2</sub> O	2.33	3.37	3.12	2.32	5.25	5.46	5.35	4.47	4.22	5.42	3.71
K <sub>2</sub> O	1.95	1.24	2.54	2.77	2.02	2.38	2.17	2.18	2.11	1.65	2.75
P <sub>2</sub> O <sub>5</sub>	0.41	0.38	0.46	0.45	0.39	0.45	0.40	0.06	0.08	0.06	0.07
LOI	3.22	2.36	2.84	2.97	4.32	2.84	4.36	1.35	1.56	2.22	1.64
Total	99.53	99.62	99.61	99.38	99.28	99.57	99.42	99.68	99.65	99.39	99.59
Mg#	48.60	52.80	50.60	52.88	49.43	50.70	48.99	55.72	54.22	52.96	53.70
La	34.49	27.43	30.64	32.34	24.77	26.92	24.38	23.27	26.60	22.52	28.17
Ce	65.98	58.54	62.13	66.01	53.01	57.80	51.68	45.03	55.73	44.51	55.71
Pr	7.37	6.48	7.30	7.64	6.21	6.97	6.11	4.44	5.29	4.42	5.56
Nd	34.49	27.43	30.64	32.34	24.77	26.92	24.38	23.27	26.60	22.52	28.17
Sm	65.98	58.54	62.13	66.01	53.01	57.80	51.68	45.03	55.73	44.51	55.71
Eu	1.42	1.19	1.32	1.39	1.32	1.49	1.30	0.56	0.66	0.52	0.64
Gd	3.50	3.17	3.59	3.53	3.65	4.12	3.55	1.91	2.18	1.86	1.97
Tb	0.47	0.43	0.48	0.48	0.51	0.58	0.50	0.30	0.33	0.29	0.29
Dy	2.30	2.16	2.47	2.38	2.67	3.06	2.63	1.70	1.75	1.67	1.53
Ho	0.42	0.39	0.45	0.44	0.50	0.57	0.50	0.34	0.34	0.35	0.30
Er	1.13	1.05	1.17	1.21	1.34	1.54	1.32	0.99	0.97	1.01	0.85
Tm	0.16	0.15	0.16	0.17	0.20	0.22	0.19	0.16	0.16	0.16	0.13
Yb	1.03	0.97	1.03	1.10	1.25	1.38	1.20	1.08	1.07	1.11	0.92
Y	11.67	11.17	12.75	12.36	13.99	15.85	13.69	10.62	10.30	10.86	8.36
Lu	0.14	0.14	0.14	0.16	0.18	0.20	0.17	0.16	0.15	0.16	0.13
Li	26.50	22.80	22.80	27.40	24.50	29.10	23.60	7.89	9.95	5.25	6.50
Be	1.92	1.55	2.03	2.19	1.32	1.43	1.23	2.20	1.97	1.69	2.07
Sc	12.60	10.40	13.60	12.60	14.80	16.70	14.30	2.29	2.47	2.52	2.39
V	115.00	95.50	101.00	118.00	181.00	196.00	178.00	15.10	25.60	13.10	39.10
Cr	93.70	86.30	106.00	95.80	89.90	96.40	84.10	6.52	10.90	17.40	22.40
Co	18.40	16.30	20.00	15.70	22.70	25.60	21.70	1.98	2.36	1.63	1.92
Ni	48.40	42.10	49.20	49.10	49.00	54.10	46.70	3.25	4.84	7.57	8.35
Cu	17.80	60.60	95.90	35.20	38.60	15.80	33.70	10.10	13.90	7.15	10.10
Zn	121.00	114.00	122.00	114.00	74.20	94.30	71.10	48.60	70.10	31.80	62.50
Ga	22.30	18.40	21.60	22.20	19.10	21.10	18.50	13.70	15.50	14.20	15.90
Rb	88.20	54.40	106.00	122.00	40.90	53.60	42.20	45.70	46.70	48.70	62.60
Sr	1 233.00	861.00	829.00	742.00	10 179.00	10 009.00	10 200.00	387.00	415.00	394.00	322.00
Zr	179.00	154.00	186.00	183.00	143.00	161.00	139.00	127.00	130.00	137.00	129.00
Nb	7.11	6.29	7.44	7.28	6.25	6.94	6.07	8.23	9.07	7.87	8.91
Mo	0.32	0.40	0.40	0.31	1.29	1.24	1.25	0.68	0.94	0.63	0.90
Cs	9.41	6.61	13.50	13.20	6.00	7.11	6.08	6.12	9.33	3.87	10.60
Ba	663.00	380.00	678.00	838.00	478.00	415.00	503.00	455.00	441.00	296.00	507.00
Hf	4.34	3.78	4.50	4.45	3.54	4.04	3.45	3.46	3.66	3.75	3.71
Ta	0.47	0.41	0.49	0.49	0.39	0.44	0.39	0.64	0.67	0.59	0.72
Pb	18.30	12.60	12.30	29.90	18.80	15.90	18.70	12.30	19.70	5.10	12.00
Th	7.48	6.17	7.81	7.79	5.39	6.13	5.33	9.95	11.00	10.50	11.60
U	1.68	1.30	1.40	1.58	1.50	1.61	1.46	1.56	1.89	1.30	1.98
La <sub>N</sub> /Yb <sub>N</sub>	24.08	20.22	21.36	21.06	14.24	14.04	14.52	15.47	17.89	14.51	22.06
δEu	1.08	0.98	0.97	1.01	0.98	0.98	0.98	0.78	0.79	0.74	0.81